Chapter 4 Mesoscopic Semiconductor Structures In recent years, advances in crystal growth techniques made it possible to realize semiconductor microstructures, which are so small that their electronic and optical	Chương 4 Cấu trúc bán dẫn meso Mesoscopic: thuộc hệ trung mô, hệ có kích thước trung bình, tức là kích thước nằm trong khoảng kích thước phân tử đến micro mét. Trong những năm gần đây, những tiến bộ trong kỹ thuật nuôi tinh thể giúp chúng ta có thể chế tạo được các vi cấu trúc bán dẫn, những cấu trúc này có kích thước quá nhỏ đến

properties deviate substantially from those of bulk materials. In these microstructures, the energetically low-lying electron and hole states are confined in one or more directions to a region of length Lc, which is still considerably larger than the lattice constant but so small that the electron envelope wave functions become quantized. Structures of this size are called mesoscopic because the confinement length Lc is intermediate between the microscopic lattice constant and the macroscopic extension of a bulk crystal. Đối với sóng điều hòa, chúng ta dùng khái niệm biên độ, đối với sóng bất kỳ có biên độ thay đổi chúng ta dùng khái niệm hàm bao. Đó là một hàm bao quanh các biên độ.	mức các tính chất quang và điện của chúng khác biệt rất nhiều so với vật liệu khối. Trong những vi cấu trúc này, các trạng thái electron và lỗ trống nằm ở mức năng lượng thấp không thể chuyển động theo một hoặc nhiều chiều nhất định, hay nói cách khác chúng (các trạng thái) bị giam cầm trong một vùng có độ dài Lc, Lc lớn hơn nhiều so với hằng số mạng nhưng vẫn còn rất nhỏ vì thế các hàm sóng bao của electron sẽ bị lượng tử hóa. Những cấu trúc ở kích thước này được gọi là các cấu trúc meso bởi vì giá trị của chiều dài giam cầm Lc nằm trung gian giữa hằng số mạng vi mô và độ giãn vĩ mô của tinh thể khối.
The best known examples of such mesoscopic semiconductor structures are quantum wells, where the electrons are confined in one space dimension. The translational motion in the plane perpendicular to the confinement direction is unrestricted. Such a quantum well, e.g. of the III—V compound semiconductor GaAs, can be realized by using molecular beam epitaxy to deposit several GaAs layers in between layers of a material with a wider band gap, such as GaxAl\-x As, with $0 < x < 0.4$. For substantially larger Al concentrations, the barrier material becomes an indirect-gap semiconductor.	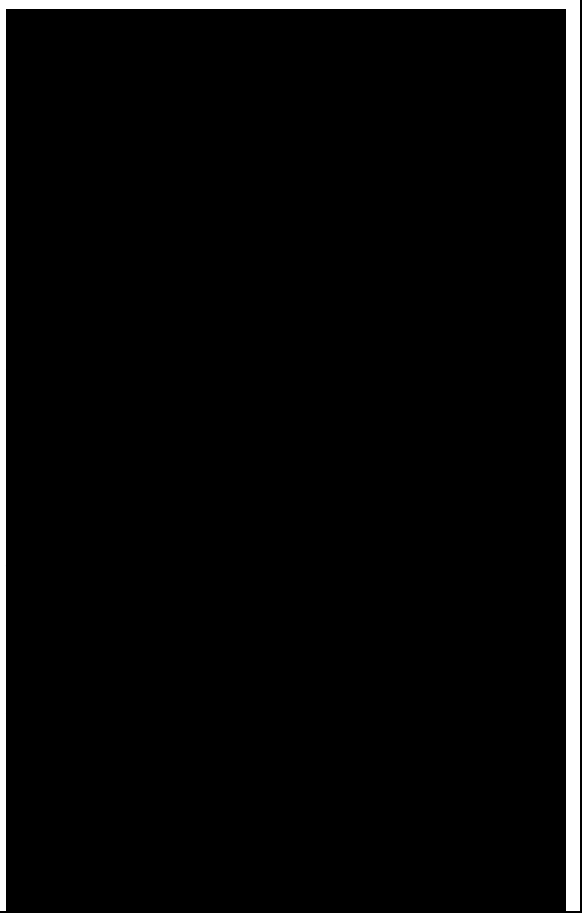

In most cases, the quantum-well structures are designed in such a way that the lowest electron and hole states are confined in the well material. These type-I structures will be discussed in more detail in this and later chapters of this book. To complete this classification, we mention here also the type-II quantum wells, where electrons and holes are confined in different parts of the structure, e.g. holes in the wells and electrons in the barriers, as in GaAs/AlAs. Type-II quantum wells will not be covered in this book.

If the free electronic motion is confined in two dimensions, the structure is called a quantum wire, and if the confinement exists in all three space dimensions, we speak of a quantum dot. The electronic and optical properties of these mesoscopic semiconductor microstructures will be analyzed throughout this book. After a general discussion of some basic quantum confinement effects, we discuss in this chapter the confinement-induced modifications of the electronic band structure in semiconductor quantum wells, which are currently the best studied quantum confined structures and can serve as a paradigm for others.

In later chapters, where we discuss elementary excitations and optical properties of semiconductors, we present the derivations and results as

much as possible in parallel for three-, two- and one-dimensional systems in order to gain some insight into the dimensional dependence of the various effects. Because in quantum dots the translational motion is completely suppressed, a separate chapter is devoted to the optical properties of quantum dots.

4.1 Envelope Function Approximation

In this section, we discuss the situation of a perfect and symmetric quantum well, where the optically excited electrons are completely confined inside the well material. In this idealized case, the envelope wave function of these electrons has to vanish at the interface between well and barrier. In the Bloch wave function, Eq. (3.26), the slowly varying plane-wave envelope for the motion perpendicular to the well has to be replaced by a quantized standing wave Zn(z):

(4.1)

In terms of the localized Wannier functions (3.44), the envelope approximation is

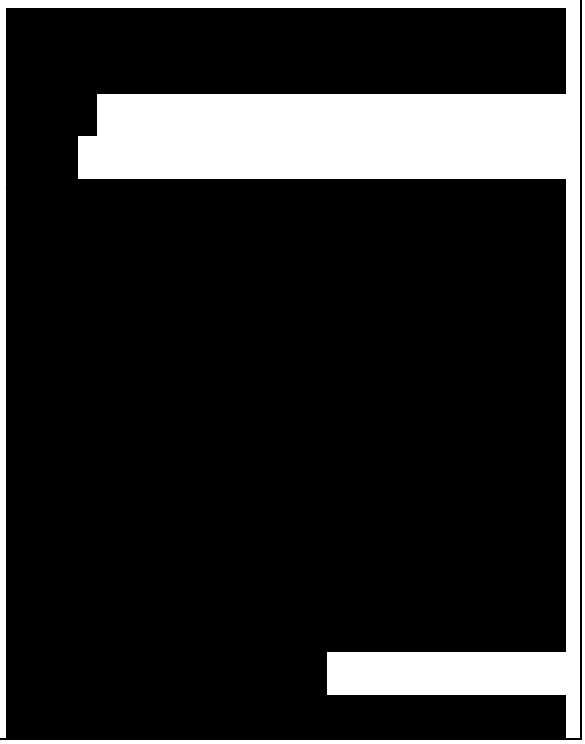

(4.2)

The energies of these quantized envelope states are very similar to those of a particle in a box. These energies are proportional to n/LC., where n =1, 2,... and Lc is the width of the well. A reduction of the size of the microstructure shifts all energies to higher values, showing clearly that the electron levels and thus the optical properties can be changed through the design of the structure.

Because of the additional

translational motion within the layer, each of the energy levels forms a subband. If the electrons populate only the lowest subband, the translational degree of freedom perpendicular to the well is completely quantized. As far as the translational electron motion is concerned, the quantum well can be approximated as a two-dimensional system under these conditions. However, in these mesoscopic structures the Bloch functions and the band structure are in first approximation still those of a bulk semiconductor. Refinements of this statement with respect to the degenerate valence bands will be given later in this chapter.

It is important to note that the Coulomb interaction in most mesoscopic systems remains essentially three-dimensional. Because the dielectric properties of the materials of the microstructure and of the barrier are normally very similar, the Coulomb field lines between two charged particles also penetrate the barrier material. This situation of a kinetically twodimensional structure where, however, the interaction potential is basically three-dimensional, is often denoted as quasi-two-dimensional.

If one creates an additional lateral confinement in a quantum well, e.g. by etching, one can obtain a quasi-one-dimensional (quasi: giả, chuẩn, gần như một chiều) quantum wire. In a rectangular quantum wire, e.g., the plane-wave envelopes for the translational motion in the two directions perpendicular to the wire axis have to be replaced by quantized

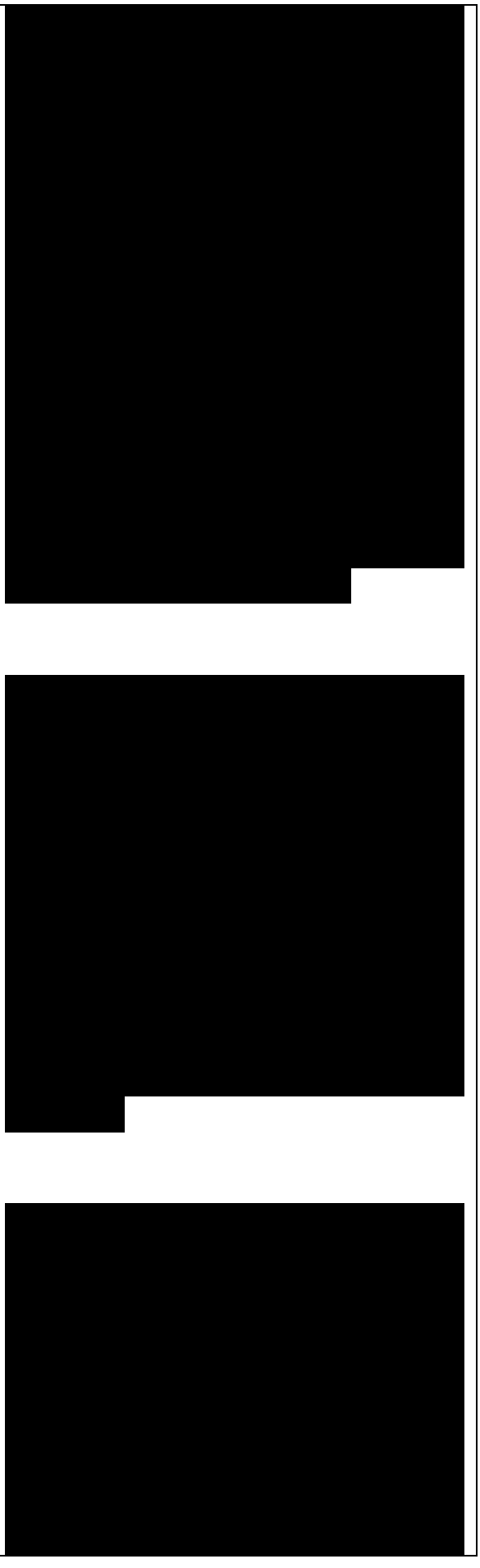

standing waves, leaving only a plane-wave factor for the motion along the wire axis. Therefore, the quantum wire is a quasi-one-dimensional system, and

(4.3)

Finally, in a mesoscopic quantum dot the electronic quantum confinement suppresses the translational motion completely, so that

It is obvious from the wave functions (4.1) - (4.4), that the free translational motion in these microstructures is described by a P-dimensional wave vector k. The sum over this wave vector is thus

If we evaluate the integral in polar coordinates we get

(4.6)

where QD is the space angle in D dimensions. If the integrand is isotropic the space angle integral yields which equals 4n in 3D, 2n in 2D, and 2 in 1D, respectively. The k integral is usually transformed in an energy integral with = E and £—2kdk = dE so that

47)

The integrand in Eq. (4.7) is called the density of states, p]j(E) oc E1?~1. Eq. (4.7) shows that pD(E) differs strongly in various dimensions p3(E) <x \f~E, po{E) = 0(E), and pi(£7) = \j\f~E. Because the absorption in the free- carrier model follows the density of states (see Chap. 5), this is a further source for the strong modifications of the optical properties resulting from the reduction of the dimensionality.

To summarize, the optical properties can be changed strongly by quantum

confinement which introduces an extra localization energy (năng lượng định xứ, năng lượng tập trung vào một khu vực cục bộ) and changes of the density of states. Later in the book we will see that also the effects due to many-body interactions are strongly dependent on the dimensionality.

4.2 Conduction Band Electrons in Quantum Wells

In this section, we extend the discussion of elementary properties of electrons in a semiconductor quantum well, whose thickness in the z direction we denote as Lc. In a type I quantum well, the energy difference AEg between the larger band gap of the barrier and the smaller band gap of the well material causes a confinement potential both for the electrons in the conduction band and for the holes in the valence band. In a GaAs- GaAlAs quantum well, e.g., the resulting well depths are AVe ~ 2AEg/3 and AVh ~ AEg/3, respectively. The potential jump occurs within one atomic layer so that one can model the quantum well as a one-dimensional potential well with infinitely steep walls. Simple analytic results are obtained if one assumes that the well is infinitely deep, so that the confinement

For the x — y plane there is no quantum confinement and the carriers can move freely. For the electrons in the nondegenerate conduction band, one can easily calculate the envelope function using the effective mass approximation for the low lying states. We shift the treatment of holes to the next section, because the symmetry reduction in a quantum well causes a mixing of the

degenerate valence bands.

The Schrodinger equation for the electron in the idealized quantum well is

Following the arguments of the preceding section, we write

where Z(z) is the mesoscopically slowly varying envelope function. We assume that the electron Hamiltonian without the confinement potential leads to the energies Ee(k) — Eg +h2(k± +k2)/2me, where me is the effective mass of the electrons in the conduction band. Replacing hkz ^ —ihd/dz we find the following equation for the standing-wave envelope Z(z):

(4.11)

This one-dimensional Schrodinger equation is that of a particle in a box with the eigenfunctions

where A and B are constants, which still have to be determined, and

(4.13)

The boundary conditions for the wave functions are

Because of the inversion symmetry of the confinement potential around z = 0, the wave functions (4.12) can be classified into even and odd states. For the even states, A = 0, and the odd states, B = 0, one gets the normalized envelope functions

(4.15)

The boundary condition (4.14) yields

(4.16)

so that

with n = 2n — 1 (for even states) and n = 2n(for odd states). Equations (4.15) - (4.17) show that the quantum confinement inhibits the free electron motion in z-direction. Only discrete kz values are allowed, leading to a

series of quantized states. We see that the lowest energy state (ground state) is even, n = 1 in Eq. (4.17), followed by states with alternating odd and even symmetry. The energy of the ground state is nothing but the zero-point energy (Apz)2/2me which arises because of Heisenberg's uncertainty relation between the localization length Az = Lc and the corresponding momentum uncertainty Apz.

Adding the energies of the motion in plane and in z-direction we find the total energy of the electron subject to one-dimensional quantum con-

(4.18)

indicating a succession of energy subbands, i.e., energy parabola h2k\/2me separated by h?n'2/2meLC,. The different subbands are labeled by the quantum numbers n.

In order to have a more realistic description, one has to use a finite confinement potential

<4'19>

The analysis closely follows that of the infinite potential case, however, the energies can no longer be determined analytically. The Schrodinger equation for the x — y motion is unchanged but the equation for the z- motion now has to be solved separately in the three regions: i) \z\ < Lc/2, ii) z > Lc/2, and iii) z < —Lc/2. In region i), the solution is given by (4.13) and in regions ii) and iii) by

c (z) = C±e±Kz z (4.20)

with

K: = =^(VC-EZ) . (4.21)

The normalization of the wave functions requires that we have to choose the exponentially decaying solutions in (4.20). Furthermore, we have to match the wave functions and their derivatives at the interfaces ±zc/2. This yields for the even states with the condition (see problem 4.2)

(4.23)

The solution of this equation gives the energy eigenvalues Ez for the even states.

The same procedure for the odd states yields

with

……(4.25)

The roots of the transcendental equations (4.23) and (4.25) have to be determined numerically. The number of bound states in the well depends on the depth of the potential well Vc. As long as Vc is positive, there is always at least one bound even state, the ground state. If more than one bound quantum confined state exists, the symmetry between the successive higher states alternates, until one reaches the highest bound state. The energetically still higher states are unbound and not confined to the quantum wells.

4.3 Degenerate Hole Bands in Quantum Wells

We have seen in the previous section, that multiple subbands occur due to the quantization of the electron motion in z-direction. For degenerate bands, one has to expect modifications of the band structure

for the inplane motion of the carriers, since the quantum confinement generally leads to a reduction of the original spherical or cubic symmetry, and thus to a removal of band degeneracies and to band mixing. We assume here — as implicitly done before — perfectly lattice matched conditions between the barrier and the well material. Generally, however, perfect lattice matching is not a necessary requirement for the epitaxial growth of heterostructures. A small mismatch of the lattice constants can often be accommodated by elastically straining one or both of the components leading to strained layer structures.

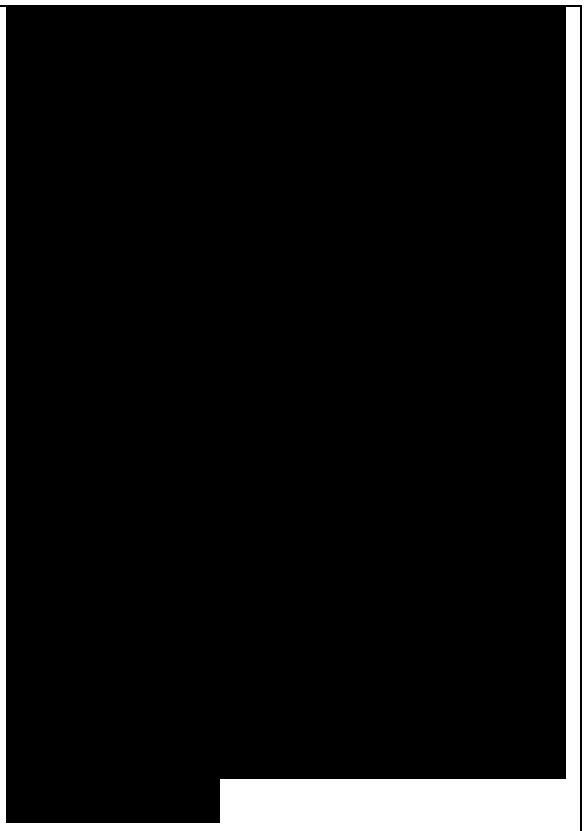

As for the electrons, we assume that an effective bulk Hamiltonian for the holes can be used for the determination of the envelope functions if one replaces hkz ^ pz = —ihd/Dz. The matrix of the hole-band Hamiltonian (3.83) for the four degenerate eigenstates J = 3/2 states with

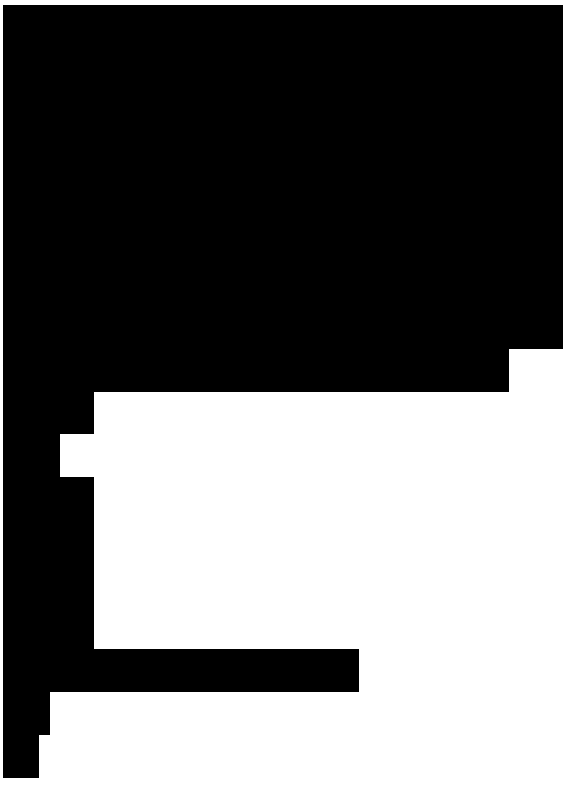

as expectation values with the envelope functions Z. For a symmetric well, (pz} vanishes between states of equal symmetry. Thus, if we neglect intersubband

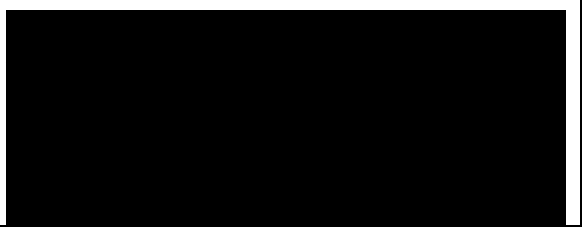

mixing, b = 0.

Note, that the light-hole Hamiltonian Hlh has, due to the finite localization energy (pi}/2mo, a higher energy than the heavy-hole Hamiltonian. Consequently, the degeneracy at k^ =0 of the bulk semiconductor material is lifted. However, according to these simple arguments, the unperturbed bands in the quantum well would cross at a finite k^ value. Interchanging the first and last row and successively the first and last column in (4.26) yields the following eigenvalue problem

Since the matrix is block diagonal, one is left with the diagonalization of a two-by-two matrix

The corresponding eigenvalues are given by

The solutions are

The resulting dispersion is shown in Fig. 4.1 for c = 0 and c = 0. We see the typical level repulsion and the state mixing in the momentum region where the dispersion cross for c = 0.

PROBLEMS

Problem 4.1: Use the effective mass approximation to calculate the electron energies.

a) for a square quantum wire with finite barrier height in two dimensions,

b) for a square quantum dot (quantum box), in which the electrons are confined in all three dimensions.

Show that increasing quantum confinement causes an increasing zero-point energy due to the

Heisenberg uncertainty principle.

Problem 4.2: Solve the Schrodinger equation for the motion of an electron in a finite potential well. Derive the transcendental equations (4.23) and (4.25) for the energy eigenvalues using the conditions of continuity of the wave function and its derivative at the boundary of the confinement potential.

Problem 4.3: Calculate the matrix (mj\H\mJ) for the J = 3/2 states using the Hamiltonian (3.83).

a) Show that J2 — J2 = J+ J_ + J_ J+).

b) Express the Hamiltonian (3.83) in terms of the operators J± = Jx ± iJy, Jz, and J2. Derive the form

(4.37)

where {Jz, J+} = }j(JxJ+ + J+Jz) and h.c. means the hermitian conjugate of the preceding term, and hkz = (pz}.

c) Calculate the matrix elements (4.26) - (4.31) using Eq. (3.108) for the action of J± on the states \J, mJ}. Note, that {J2} = J (J + 1).

Chapter 5
Free Carrier Transitions

In a typical semiconductor, the gap between the valence band and the conduction band corresponds to the energy hw of infrared or visible light. A photon with an energy hw > Eg can excite an electron from the valence band into the conduction band, leaving behind a hole in the valence band. The excited conduction-band electron and the valence-band hole carry opposite charges and interact

via the mutually attractive Coulomb potential. This electron-hole Coulomb interaction will naturally influence the optical spectrum of a semiconductor. However, in order to obtain some qualitative insight, in a first approximation we disregard all the Coulomb effects and treat the electrons and holes as quasi-free particles.

5.1 Optical Dipole Transitions

Generally, electrons in the bands of a semiconductor are not in pure states but in so-called mixed states. Therefore, we have to extend the quantum mechanical method used to calculate the optical polarization in comparison to the treatment presented in Chap. 2. While pure states are described by wave functions, mixed states are described by a density matrix. In this chapter, we again use the technique of Dirac state vectors | Ak) with the orthogonality relation
and the completeness relation

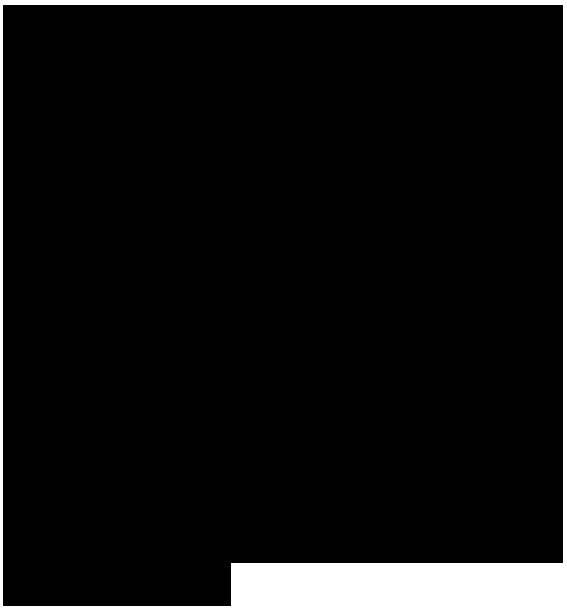

The state vectors |Ak) are eigenstates of the crystal Hamiltonian (3.5), which we now denote by Ho:
Ho|Ak) = £A(k)|Ak) = hex,klAk) . (5.3)

As usual, Eq. (5.3) is transformed into the Schrodinger equation in real-space representation by multiplying (5.3) from the left with the vector (r|. The Schrodinger wave function ^A(k, r) for the state | Ak) is just the scalar product
^A(k, r) = (r|Ak) , (5.4)

i.e., the Bloch wave function (3.26)

for the band A.

The Hamiltonian of electrons in a crystal can be obtained in this representation by multiplying Ho from the left and right with the completeness (tập hợp đầy đủ trạng thái) relation (5.2)

Ho = £ |A,k,)(A,k,|Ho £ ^(Ak . (5.5)

Using Eqs. (5.3) and (5.1), we find the diagonal representation

Ho = h£ £A,k|Ak)(Ak| . (5.6)

The action of the Hamiltonian (5.6) on an arbitrary state vector can easily be understood. The "bra-vector" (Ak| projects out that part which contains the state with the quantum numbers A, k represented by the "ket-vector" | Ak).

As discussed in Chap. 2, the dipole interaction with the light is described by

HI = -er E(t) = -dE(t) , (5.7)

where er = d is the projection of the dipole moment in the direction of the electromagnetic field. Using the completeness relation twice yields

HI = -e E (t) £ rAA' (^, k)|AV)(Ak| , (5.8)

with

To compute the dipole matrix element, we assume only interband transi-tions, X = X', and use the same trick as in Eqs. (2.26) and (2.31) to get

……..(5.10)

Inserting

and using the fact that the momentum operator is diagonal in the r-representation, we get

(X'k'|p|Xk) = f d3r^*y (k', r)p^A(k, r) . (5.11)

As in Sec. 3.3, we expand the Bloch functions uA(k, r) into the complete set un(0, r). Using only the leading term of the k • p-result, Eq. (3.66), we get

<Mk,r. (5.12)

Inserting (5.12) into (5.11) yields

……

where the additive fok results from commuting p and exp(ik • r). Now we split the integral over the entire crystal into the unit-cell integral and the sum over all unit cells, Eq. (3.38), replace r ^ r + R„, and use Eq. (3.27), to get 9 h 51

Fig. 5.1 Schematic drawing of conduction and valence bands and an optical dipole transition connecting identical k-points in both bands.

Since the unit-cell integral yields the same result for all unit cells, we can take it out of the summation over the unit cells, which then yields Sk,k', and Eq. (5.14) becomes

(A'k'IplAk) = ^- J d3r ii*x,(0,r)piix(0,r) = dkjk/pA'A(0) , (5.15)

where the term <x hk disappeared because of the orthogonality of the lattice periodic functions and our A = A' requirement.

The ^-function in Eq. (5.15) shows that the optical dipole matrix element couples identical k-states in different bands, so that optical transitions are "perpendicular" if plotted in an energy-wave-number diagram, as in Fig. 5.1. The dipole approximation is equivalent to ignoring the photon momentum in comparison to a typical electron momentum in the Brillouin

zone.

Collecting all contributions to the dipole matrix element, we get

(5.16)

(5.17)

optical dipole matrix element

where we used Eq. (5.16) for k = k = 0 to lump all parameters into

(5.18)

For the cases of two parabolic bands with effective masses m\ and my and dispersions

(5.19)

the optical dipole matrix element is

(5.20)

Except for the ^-function the k-dependence of the dipole matrix element can often be neglected in the spectral region around the semiconductor band edge. The k-dependence is usually important only if the variation over the whole first Brillouin zone is needed, as in Kramers-Kronig transformations or computations of refractive index contributions.

5.2 Kinetics of Optical Interband Transitions

In order to keep the following treatment as simple as possible, we now make a two-band approximation by restricting our treatment to one valence band v and one conduction band c out of the many bands of a real semiconductor, i.e., A = c, v. This two-band model is a reasonable first approximation to calculate the optical response of a real material if all the other possible transitions are sufficiently detuned with regard to

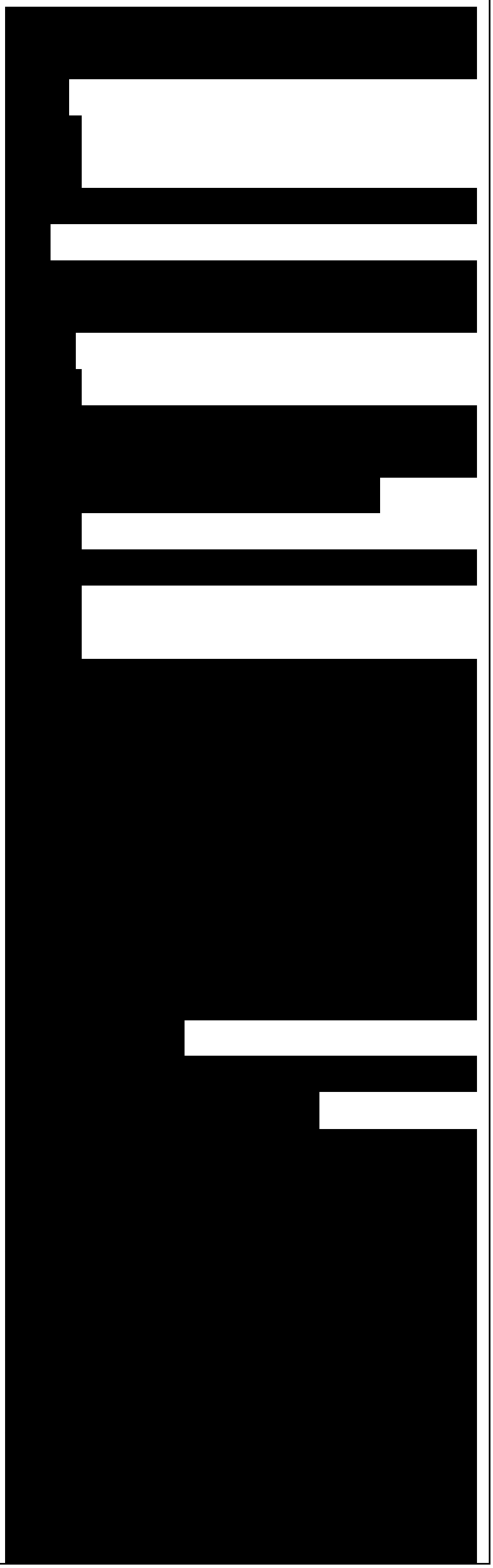

the frequency region of interest. We will treat first quasi-D-dimensional semiconductors, followed by an extension to quantum confined semiconductors with several subbands.

5.2.1 Quasi-D-Dimensional Semiconductors

Quasi: giả, chuẩn, gần

To simplify our analysis even further, we ignore the ^-dependence of the dipole matrix element and write the interaction Hamiltonian in the form

(5.21)

showing that different A-states are not mixed as long as we ignore the Coulomb interaction between the carriers.

Evaluating the summation over the band indices yields

(5.22)

where d*cv = dvc has been used. For our subsequent calculations it is advan-tageous to transform the Hamiltonian into the interaction representation

(5.23)

where h.c. denotes the Hermitian conjugate of the preceding term.

The single-particle density matrix pk(t) of the state k can be expanded into the eigenstates \ Ak)

(5.24)

single-particle density matrix for the state k

The equation of motion for the density matrix is the Liouville equation d i

-jPkit) = ~-[Hk , Mt)] (5.25)

which is written in the interaction representation as d i

with

Inserting Eqs. (5.23) and (5.27) into

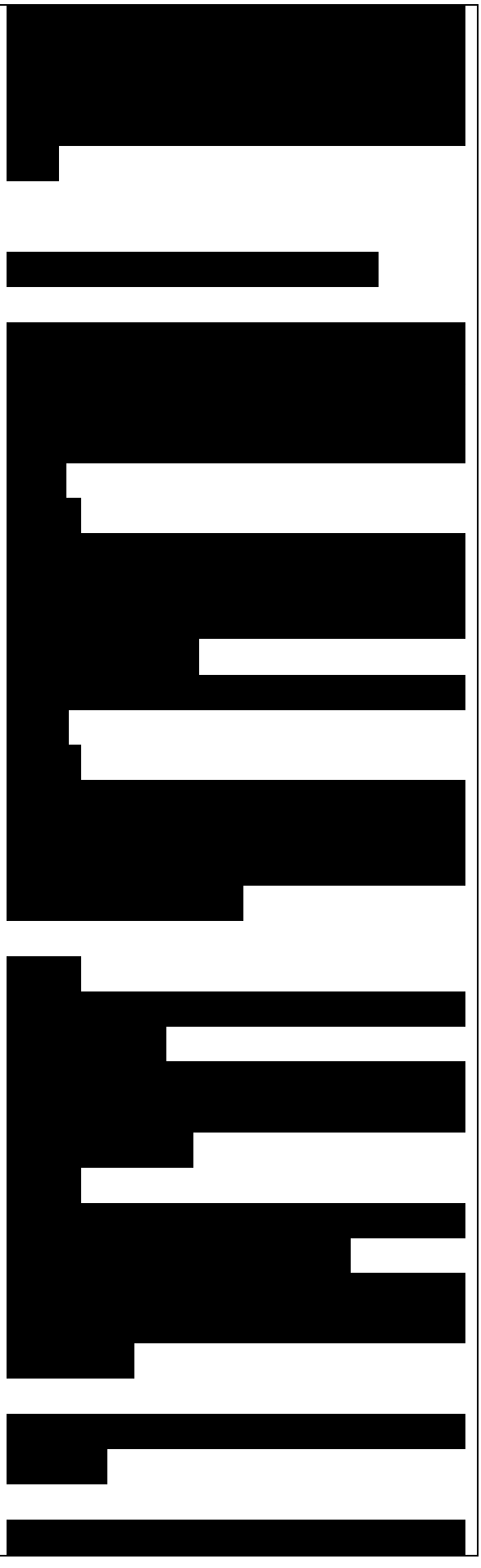

(5.26), we get
(5.28)
Taking the matrix element PiniKt) = {ck\pint (t)\vk)
of Eq. (5.28) yields

Eq. (5.30) shows that the off-diagonal elements pcv of the density matrix for the momentum state k couple to the diagonal elements pcc, pvv, of the same state. The coupling between different k-values is introduced when we also include the Coulomb interaction among the carriers.
The diagonal elements of the density matrix PAA give the probability to find an electron in the state \Ak), i.e., PAA is the population distribution of the electrons in band A. From Eq. (5.28) we obtain

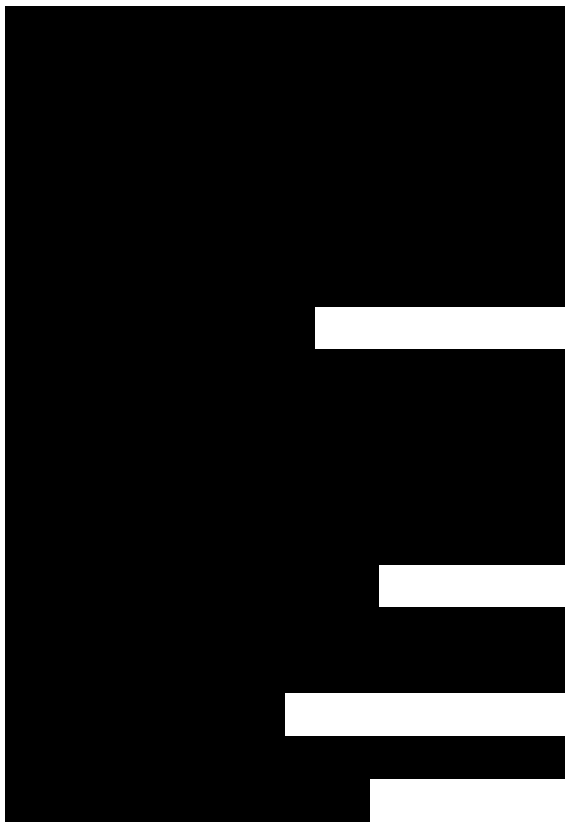

In Eqs. (5.31) and (5.32), we used pcv = p*vc, which follows from Eq. (5.30).

5.2.2 Quantum Confined Semiconductors with Subband Structure

In the Wannier function representation (4.2), the electron state is characterized by a band index i and by an envelope index v in which we collect the quantum number n of the confined part of the envelope, and the D- dimensional wave vector k of the plane wave part of the envelope. For a quantum well, e.g., the envelope £M(r) would stand for CM(z)exp(ik|| • r\\)/L. The optical matrix element is

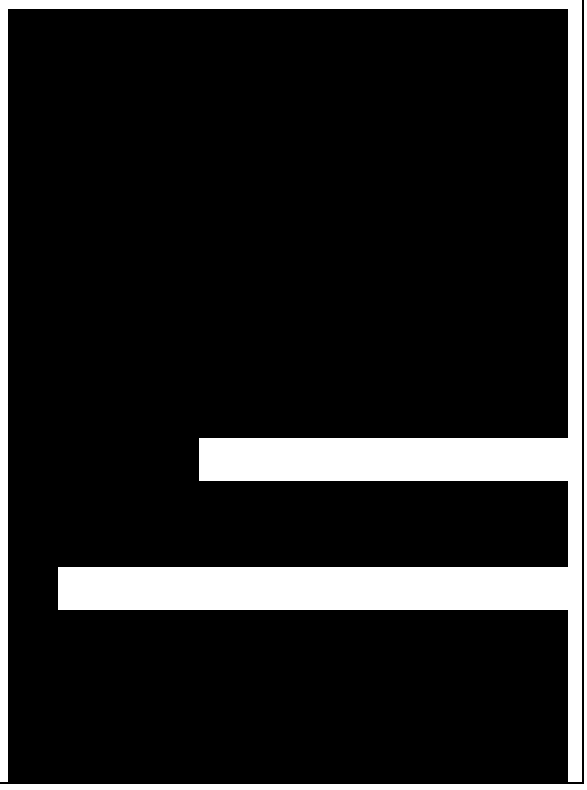

With the substitution r ^ (r — Rn) + Rn the integral over the Wannier functions yields approximately
where rij = J d3rw* (r)rwj (r) is the matrix element between Wannier func-tions localized at the same lattice site. Approximating the sum

over all lattice sites by an integral V I d3r, where Vn is the volume of a unit cell, we finally get …… (5.34)

This result holds if the envelope function is much more extended than the Wannier function. The first term represents the optical matrix element of the interband transitions i = j, usually for transitions between states of one of the valence bands and the conduction band. For a quantum well, the integral over the envelope functions would yield the momentum selection rule k| = k| and the subband selection rule. Often the equal subband contributions n = m are dominant. The second term describes the matrix element of the infrared intersubband transitions.

The density matrix for a mesoscopic semiconductor structure with several subbands is
P(t) = 53 Pi,v;j,»(t)\iv)(jP\ . (5.35)
From the Liouville equation we obtain the equation of motion as
(5.36)

where diyVis the projection of the dipole matrix element in field direction. In order to study a specific system, one has to insert the appropriate dipole matrix element, Eq. (5.34), for the optical transitions of interest.

Equations (5.30) - (5.32) for the two-band system, and Eq. (5.36) for the multi-band system, describe the interband kinetics of the free carrier model. In later chapters of this book, many-body effects due to the

interaction between the excited carriers will be incorporated into these equations. However, before we discuss the interaction processes in detail, we analyze two important limiting cases of the noninteracting system in this chapter: i) coherent optical interband transitions and ii) the case of a quasi-equilibrium electron-hole plasma.

Coherent optical interband transitions are realized at least approximately in experiments using ultra-short optical pulses. Here, the carriers follow the laser field coherently, i.e., without significant dephasing. Examples of such coherent optical processes are the optical Stark effect, ultrafast adiabatic following, photon echo, and the observation of quantum beats.

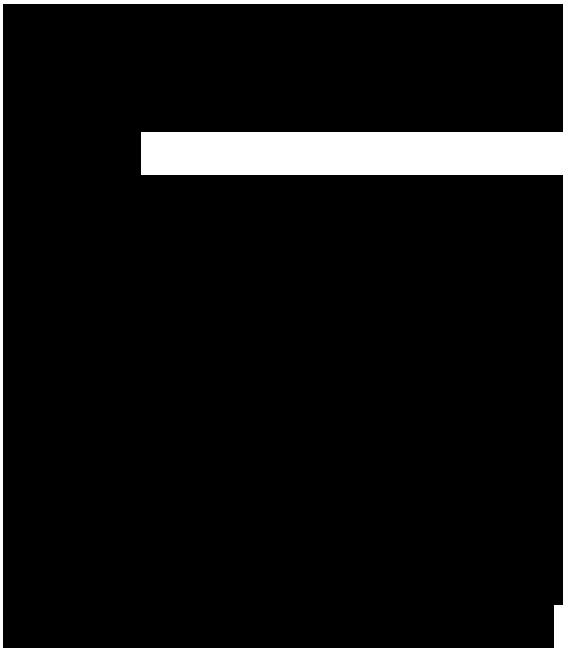

A quasi-equilibrium situation is typically reached in experiments which use stationary excitation, or at least excitation with optical pulses which are long in comparison to the carrier scattering times. Under these conditions the excited carriers have sufficient time to reach thermal quasi-equilibrium distributions within their bands. “Quasi-equilibrium” means that the carriers are in equilibrium among themselves, but the total crystal is out of total thermodynamic equilibrium. In total equilibrium, there would be no carriers in the conduction band of the

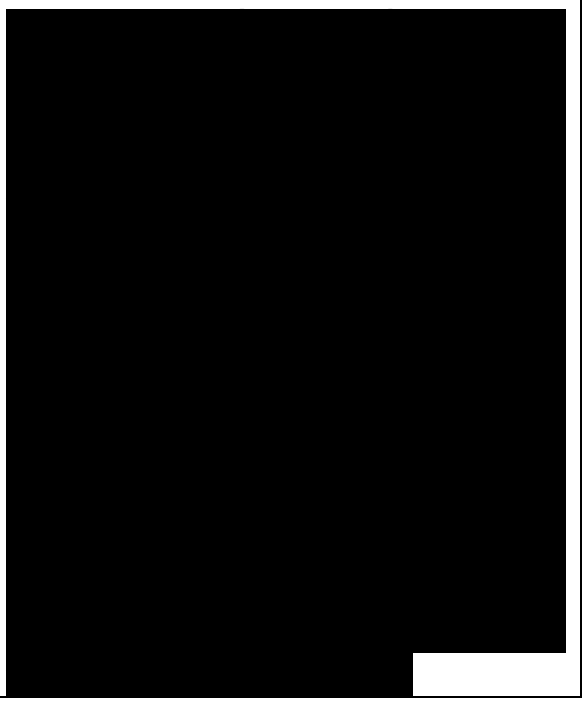

semiconductor.

5.3 Coherent Regime: Optical Bloch Equations

In this section, we discuss the interband kinetics for semiconductor systems for the coherent regime assuming a two-band system. The extensions to microstructures with several subbands is straightforward, using the results of the last subsection.

We simplify the free-carrier interband kinetic equations (5.30) - (5.32) by assuming an electromagnetic field in the form

…(5.37)

where Eo is a slowly varying amplitude. Using

(5.38)

and taking into account only the resonant terms (rotating wave approximation, RWA) proportional to exp[±i(w — ec,k + ev,k)t], we can write the interband equations as

(5.39)

Here, we introduced the detuning

(5.41)

and the Rabi frequency

(5.42)

With the assumption dcv = dvc the Rabi frequency is real.

A helpful geometrical visualization of the kinetics described by Eqs. (5.39) and (5.40) is obtained if we introduce the Bloch vector, whose

(5.43)

From Eqs. (5.39) and (5.40) we obtain the following equations of motion for the Bloch-vector components

coherent optical Bloch equations

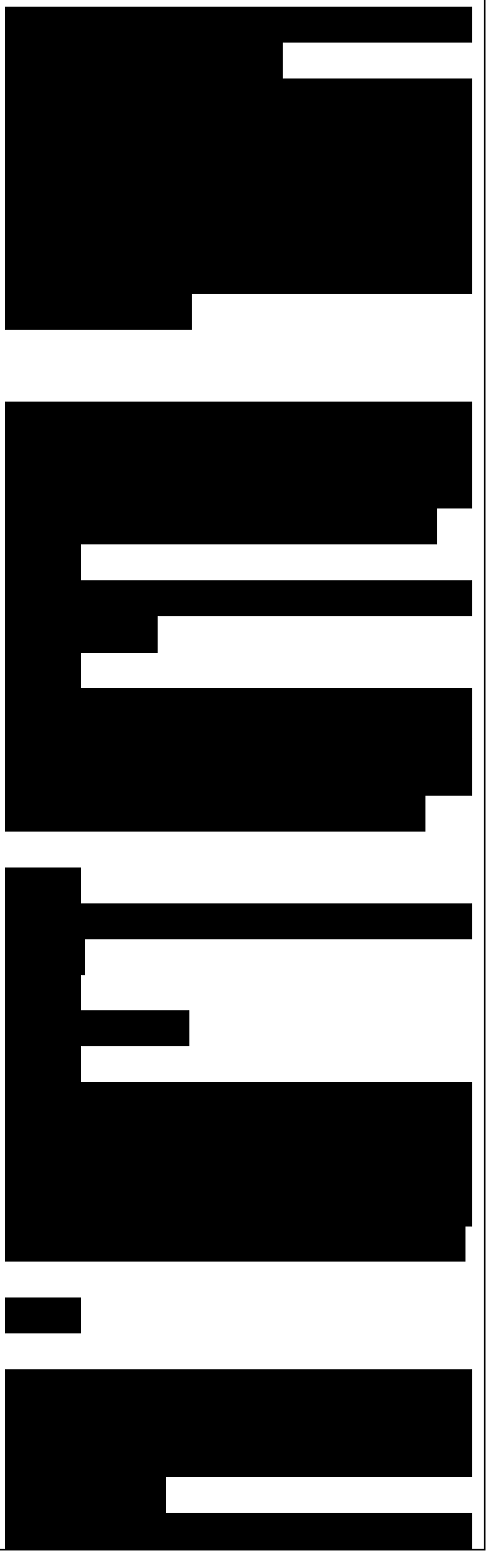

These coherent Bloch equations can be written as single vector equation

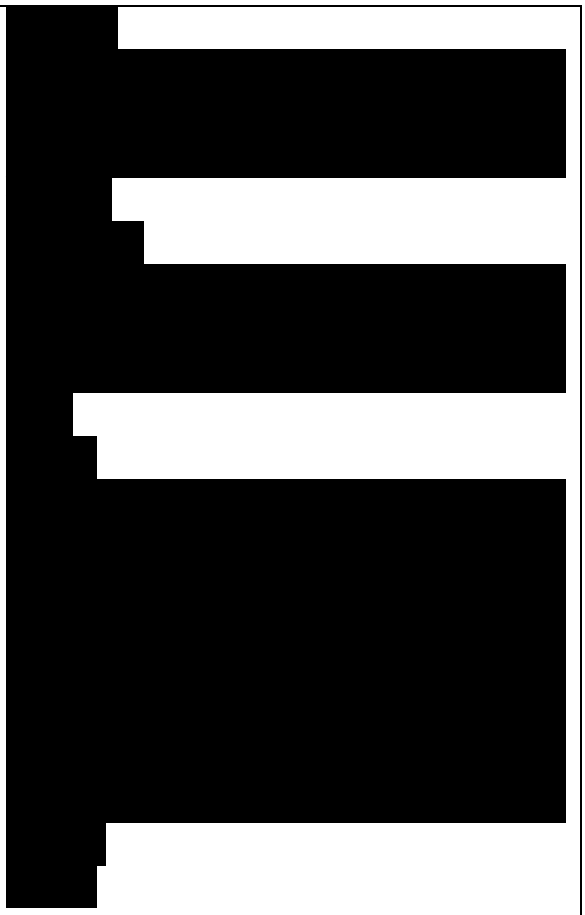

Where
is the vector of the rotation frequency, and the e* are Cartesian unit vectors. It is well known from elementary mechanics that
……..(5.47)
describes the rotation of the vector r around u, where the direction of u is the rotation axis and w is the angular velocity. Using the analogy of Eqs. (5.45) and (5.47) one can thus describe the optical interband kinetics as a rotation of the Bloch vector. The length of the vector remains constant, and since in the absence of a field

the Bloch vector for coherent motion is a unit vector with length one.

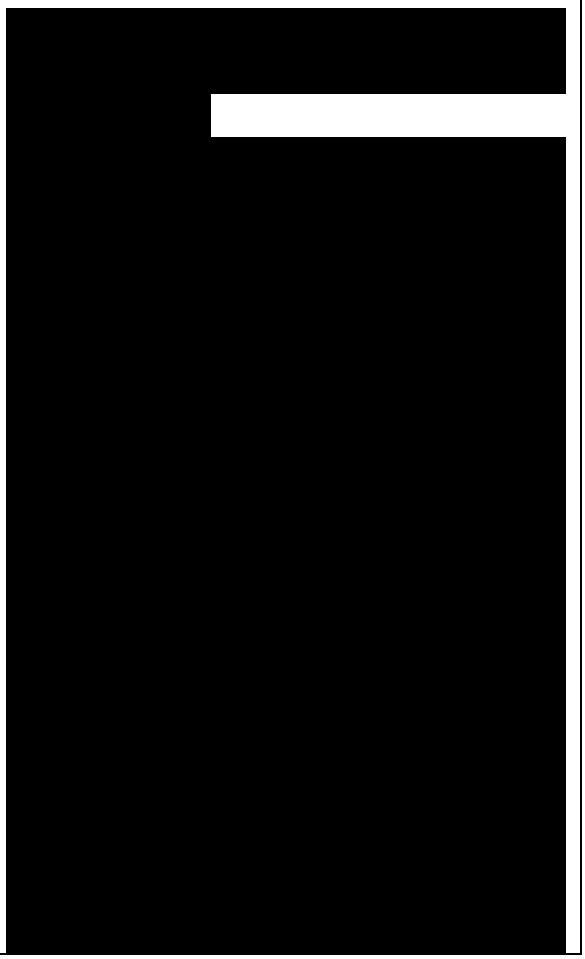

If the system is excited at resonance, vk = 0, then U rotates under the influence of a coherent field around the ei axis in the z — y plane. Starting in the ground state, U3(t = 0) = —1, a light field rotates the Bloch vector with the Rabi frequency around the -ei axis. After the time wRt = n/2 the inversion U3 is zero, and the polarization reaches its maximum U2 = 1. After wRt = n the system is in a completely inverted state, U3 = 1, and it returns after wRt = 2n to the initial state, U3 = —1. Such a rotation is called Rabi flopping. A light pulse of given duration turns the Bloch vector a certain angle. This is the basic idea for the phenomenon of photon echo.

With a finite detuning v > 0, e.g., a z-component is added to the rotation axis, so that the rotations no longer connect the points U3 = 1 and U3 = —1.

For a more realistic description, we have to add dissipative terms to the Bloch equations. Here, we simply introduce a phenomenological damping of the polarization, i.e., we assume a decay of the transverse vector components Ui and U2 with a transverse relaxation time T2. Additionally, we take into account that the inversion U3 decays, e.g., by spontaneous emission, to the ground state U3 = —1. This population decay time is the longitudinal relaxation time Ti. It is an important task of the many-body theory to derive the relaxation times from the system interactions. Including these relaxation times, the Bloch equations take the form

(5.49)

optical Bloch equations with relaxation

To get a feeling for the decay processes described by the relaxation rates in Eqs. (5.49), let us assume that a short pulse with the area n/4 has induced an initial maximum polarization

…… (5.50)

To study the free induction decay, i.e., the decay in the absence of the field,

Fig. 5.2 Schematic drawing of the rotation of the Bloch vector for excitation with a rectangular pulse of area n/2 pulse and a finite detuning for T2 ^ Ti.

we take WR = 0 in (5.49) and obtain (5.51)

with the solution
(5.52)
Eq. (5.52) shows how T2 causes a decay of the polarization while it rotates with the detuning frequency vk around the z-axis. The polarization spirals from the initial value to the stable fix point Ui = U2 = 0, if we disregard the inversion decay. Because of the band dispersion included in vk, the polarization of electron-hole pairs with different k-values rotates with different rotation frequencies. If one applies after a time T a second light pulse, which causes a rotation of the Bloch vector by n around the ei axis, one keeps the Bloch vector in the x — y plane (Fig. 5.2). A polarization component which had rotated at time T by an angle a will find itself again separated from the origin after the n pulse, this time by —a. Since all polarization components continue to rotate around e3 with Vk, they all return to the origin after the time 2t . The coherent superposition of all polarization components causes the emission of a light pulse, the photon echo pulse. Naturally, the intensity of the photon echo depends on the dephasing time (thời gian electron dẫn mất đi đặc tính lượng tử của nó) and decreases as

By varying the time delay T between the two pulses, one can thus use a

photon echo experiment to measure the dephasing time T2.

5.4 Quasi-Equilibrium Regime: Free Carrier Absorption

The assumption of quasi-thermal distributions of the electrons in the conduction band and of the holes in the valence band provides a significant shortcut for the analysis of the optical response, since the diagonal elements of the density matrix do not have to be computed, but are given by thermal distribution functions. We discuss some aspects of carrier-carrier scattering and the mechanisms leading to a quasi-equilibrium situation in later chapters of this book. Here, in the framework of the free carrier model we simply postulate this situation. As is well known, the thermal equilibrium distribution for electrons is the Fermi distribution

(5.54)

where = l/(kBT) is the inverse thermal energy and kB is the Boltzmann constant. The Fermi distribution and its properties are discussed in more detail in the following Chap. 6. For the present purposes, it is sufficient to note that the chemical potential Mx is determined by the condition that the sum k fx,k yields the total number of electrons Nx in a band A, i.e.,

where we assume that the summation over the two spin directions is included with the k-summation. In total equilibrium and for thermal energies, which are small in comparison to the band gap, the

valence band is completely filled and the conduction band is empty, i.e.,

where N is the number of atoms.

The quasi-equilibrium approximation is a significant simplification in comparison to the full set of Bloch equations, since we do not have to solve Eqs. (5.31) and (5.32) for the diagonal terms. Inserting the distribution functions (5.54) into the RHS of Eq. (5.30), expressing the field through its Fourier transform, Eq. (2.16), and integrating over time yields (5.56)

The optical polarization is given by

P(t) = tr[p(t)d] = tr[pint(t)dint(t)] , (5.57)

where tr stands for trace, i.e., the sum over all diagonal matrix elements:

(5.58)

and

(5.59)

Since

(5.60)

and

(5.61)

(5.62)

Mec,k - ev,k + U + iY)_ optical susceptibility for free carriers

According to Eq. (1.53), the absorption spectrum is determined by the imaginary part of x(^)

(5.63)

Since it is possible to evaluate Eq. (5.63) for different dimensionalities D of the electron system, we will give the result for the general case. As discussed in Chap. 3, it is often possible to approximate the band energies ec,k and ev,k by quadratic functions around the band extrema.

Unless noted otherwise, we always assume that the extrema of both bands occur at the center of the Brillouin zone, i.e., at k = 0. Such semiconductors are called direct-gap semiconductors. Introducing the effective masses mc and mv for electrons in the conduction band and valence band, respectively, we write the energy difference as
(5.64)

Since the valence-band curvature is negative, we have a negative mass for the electrons in the valence band, mv < 0. To avoid dealing with negative masses, one often prefers to introduce holes as new quasi-particles with a positive effective mass
mh = -mv . (5.65)

In the electron-hole representation, one discusses electrons in the conduction band and holes in the valence band. The probability fh,k to have a hole at state k is given as
fh,k = 1 - fv,k . (5.66)

The charge of the hole is opposite to that of the electron, i.e., +e. Eq. (5.65) implies that the energy of a hole is counted in the opposite way of the electron energy, i.e., the hole has minimum energy when it is at the top of the valence band. To emphasize the symmetry in our results, we rename the conduction-band mass mc ^ me, fc ^ fe, and understand from now on that the term electron is used for conduction-band electrons and hole for valence-band holes, respectively. In the electron-hole

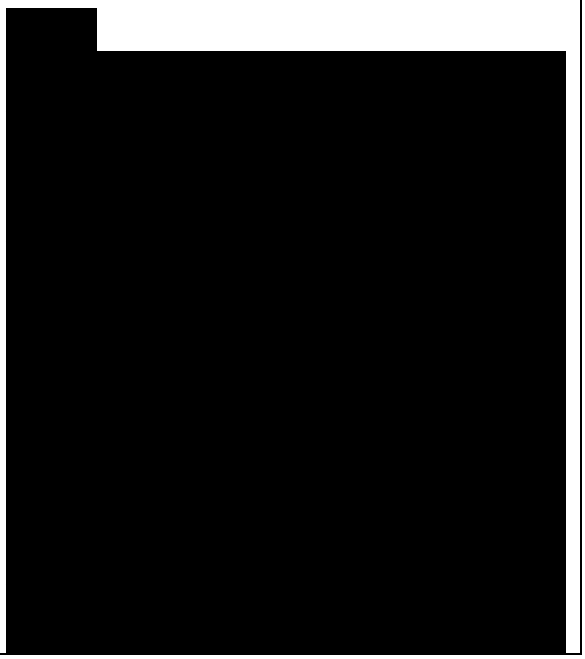

notation, the free carrier absorption (5.63) is

Furthermore, we write the energy difference as

(5.68)

where

(5.69)

is the reduced electron-hole mass.

In order to proceed with our evaluation of the absorption coefficient for electrons with D translational degrees of freedom, it is useful to convert the sum over k into an integral. Following the steps in Eqs. (4.5) - (4.7) we evaluate the k-summation in Eq. (5.67) to obtain

(5.70)

In Eq. (5.70), we have replaced the ratio LD/L3 by 1/L3C-D, where Lc denotes again the length of the system in the confined space dimensions, see Chap. 4. Furthermore, we introduced

(5.71)

In the energy-conserving ^-function, we included also the zero-point energy, which for ideal confinement (infinite potential) is

for the (3 — D) confined directions (see problem 5.2). Taking the electron- hole-pair reduced-mass energy

" (5'73)

as the integration variable, we can evaluate the integral in Eq. (5.71) with

(5-74)

as

(5.75)

where

(5.76)

The final integral in Eq. (5.75) is

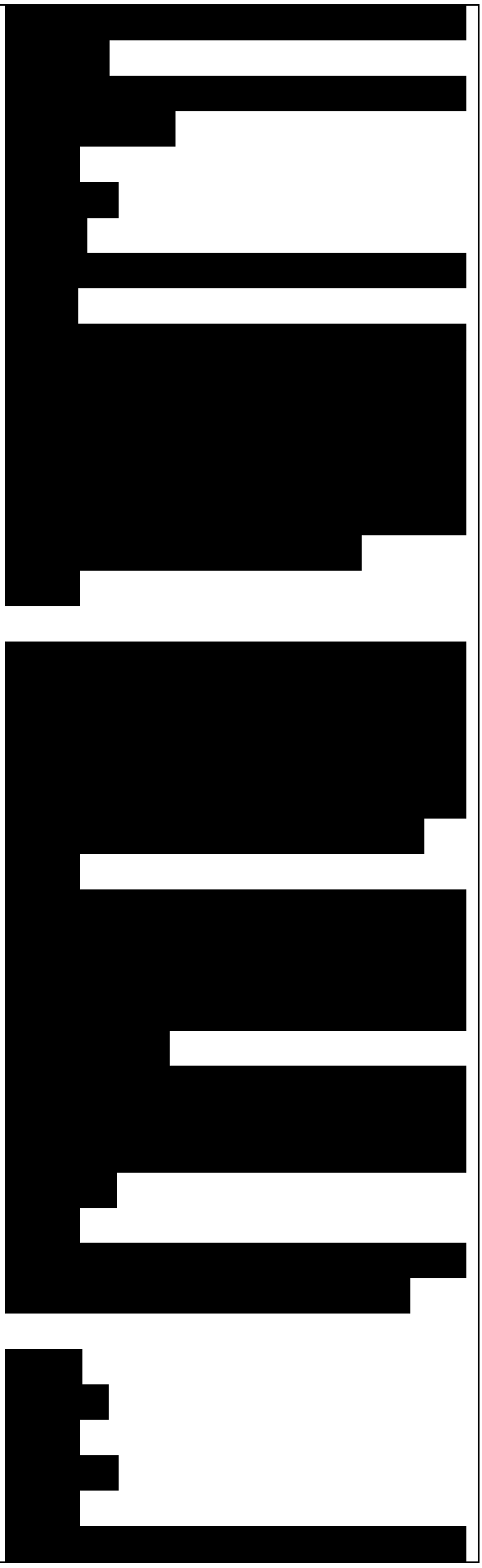

easily evaluated yielding

(5.77)

where 0(x) is again the Heavyside unit-step function and

(5.78)

with

The factor A(w) in (5.77) is often referred to as band-filling factor. Inserting the result for S(u) into Eq. (5.70), we obtain for the absorption coefficient

(5.80)

absorption coefficient for free carriers where we introduced the energy Eo = h2/(2mra0) and the length ao = h2eo/(e2 mr) as scaling parameters, and

To discuss the resulting semiconductor absorption, we first consider the case of unexcited material, where fe(u) = fh(^) = 0, i.e., A(w) = 1. The absorption spectra obtained from Eq. (5.80) for this case are plotted in Fig. 5.3. The figure shows that in two-dimensional materials the absorption sets in at Eg + Eg like a step function, while it starts like a square root ^Jfku — Eg in bulk material with D = 3, and it diverges like 1/\JTILU — Eg — EQ1^ for D = 1. The function S(iv) is just the density of states. If we considered not strictly two- or one-dimensional conditions, but a quantum well or quantum wire with a finite thickness, the density of states would exhibit steps corresponding to the quantization of the electron motion in the confined space dimensions. The first step, which is all that we have taken into

account, belongs to the lowest eigenvalue. Further steps corresponding to higher energy eigenvalues in the confined direction would belong to higher subbands.

As mentioned earlier, through optical pumping or injection of carriers, one may realize a situation with a finite number of electrons and holes. In this case, one speaks about an excited semiconductor, where the band-filling factor A(w), Eq. (5.78), differs from one. Using the properties of the Fermi functions, one can rewrite A(w) as (see problem 5.1)

(5.82)

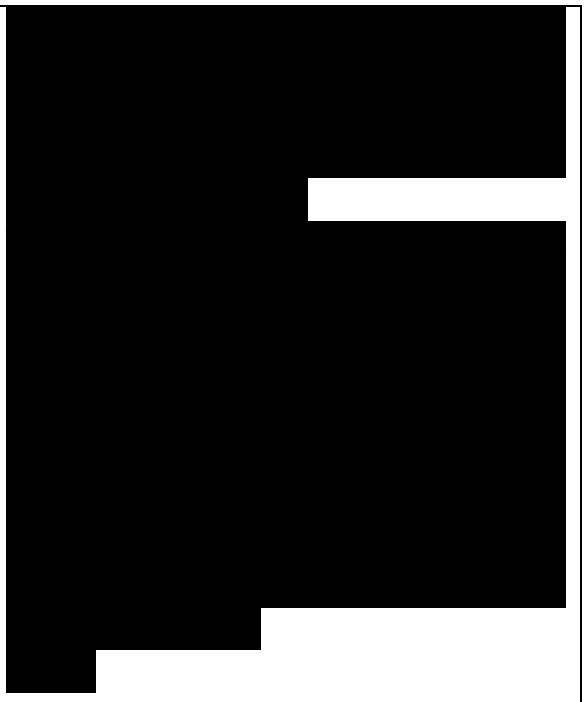

where we introduced the total chemical potential j as

(5.84)

we see that the prefactor of the tanh term in Eq. (5.82) is strictly positive, varying between 0.5 and 1. However, tanh(x) changes its sign at x = 0. The band-filling factor, and therefore the optical absorption, can become negative if p > 0 and

Eg < fau < Eg + p .(5.85)

Examples of the density-dependent absorption spectra for one-, two-, and three-dimensional free carrier systems are plotted in Figs. 5.4, 5.5, and 5.6, respectively.

As the electron-hole densities are increased, the carrier distributions gradually become more and more degenerate with positive chemical potential p/kBT. In most semiconductor systems, the effective mass of the holes is more than three times larger than that of the electrons. Consequently, the valence band

density of states is very large and the holes remain non degenerate up to rather large densities. For the highest densities in Figs. 5.4 - 5.6, the absorption becomes negative in the spectral region above the band gap, i.e., light with these frequencies is amplified, it experiences gain rather than loss (absorption).

The appearance of optical gain in the electron-hole system is the basis of semiconductor lasers, whose basic operational principles are discussed later in this book. It is interesting to compare the spectral properties of the gain for the different effective dimensionalities of the carrier system. Due to the vanishing density of states at the band gap, in a three-dimensional system (Fig. 5.6), the gain gradually increases with increasing energy and peaks at an energy between the band gap and the total chemical potential of the carrier system. Due to the step-like density of states in a two dimensional system (Fig. 5.5) we always have the gain maximum directly at the band gap, only the spectral region of optical gain increases with increasing carrier density. In the one-dimensional carrier system of Fig. 5.4, we see a very sharply peaked gain right at the band gap whose amplitude increases with increasing carrier density.

For many applications one would often prefer the gain properties of the one-dimensional system unless a broad spectral gain band width is needed, e.g., for short-pulse generation. Anyway, the strong gain modifications caused by changing the effective dimensionality of the carrier system are one of the main motives of

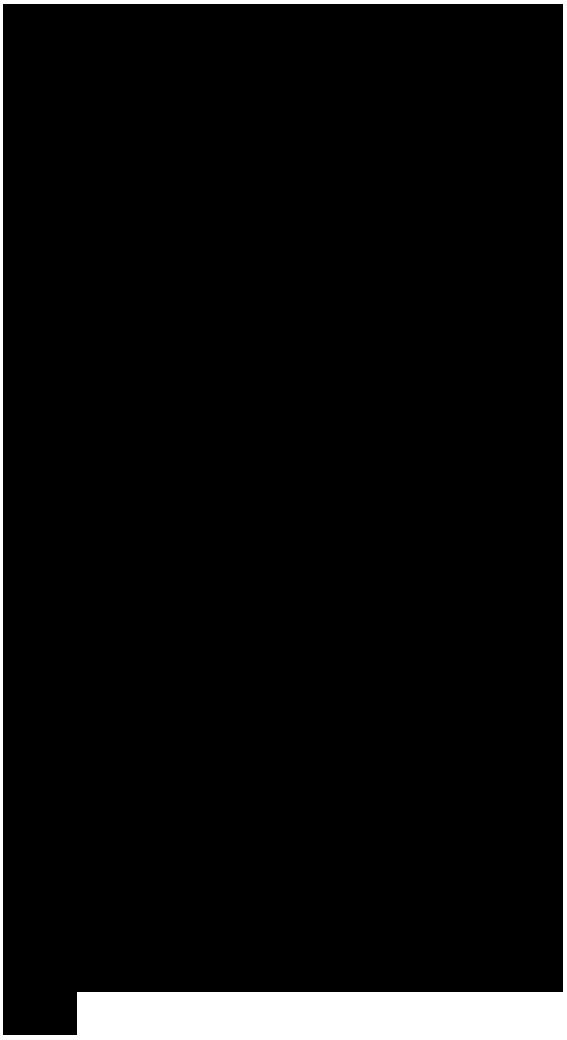

the ongoing research and development efforts in the area of low-dimensional semiconductor structures.

The density-dependent absorption spectra shown in Figs. 5.4 - 5.6 are the first example of optical nonlinearities which we discuss. The effects included in our present treatment are usually referred to as band-filling nonlinearities. Throughout this book we will encounter a variety of different sources for optical semiconductor nonlinearities.

PROBLEMS

Problem 5.1: Solve the coherent Bloch equations (5.44) for the resonant case, Vk = 0, in the form

Problem 5.2: Show that

Hint: Use tanh(x) = (ex — e x)/(ex + e x).

Problem 5.3: Calculate the onset of the absorption due to the second subband in a quasi-two-dimensional semiconductor well.

Problem 5.4: Use the Liouville equation to derive Eq. (5.36) for the multisubband quantum-well structure.

Chapter 6

Ideal Quantum Gases

As an introduction to the quantum mechanical analysis of many particle systems, we discuss in this chapter some properties of ideal quantum gases. An ideal gas is a system of noninteracting particles that is nevertheless in thermodynamic equilibrium. We analyze these systems in some detail to get experience in working with creation and destruction operators and also because we need several of the results

obtained in later parts of this book.

An elementary particle with spin $s = h(n + 1/2)$, $n = 0,1, 2,...$, is called a Fermion, while a particle with $s = hn$ is called a Boson, see also Appendix A. The Pauli exclusion principle states that for Fermions it is forbidden to populate a single-particle state more than once. This feature is incorporated into the Fermi creation and destruction operators. For example, if the same Fermi destruction operator acts on the same state more than once, it always yields zero. Bosons, on the other hand, do not obey the exclusion principle, so that no limitation of the occupation of any quantum state exists. We discuss in this chapter, how these differences result in completely different statistical properties of a gas of Bosons or Fermions.

The general method of field quantization, the so-called second quantiza-tion, is summarized in Appendix A both for Fermion and Boson systems. In this and the following chapter, we put a hat on top of operators in second quantized form, such as $\hat{n}$ for the particle number operator, to distinguish them from the corresponding c-numbers.
In order to describe quantum mechanical systems at finite temperatures, we need the concept of ensemble averages. Such averages are computed using the statistical operator $\hat{\rho}$ which is defined as
statistical operator for grand-canonical ensemble

Equation (6.1) defines the statistical operator for a grand-canonical ensemble with a variable number of particles. The expectation value (Q) of an arbitrary operator Q in that ensemble is computed as

(Q) — tr p Q. (6.2)

The trace of an operator Q can be evaluated using any complete orthonormal set of functions \n) or \l), since

tr Q — 53(l\Q\l) — 53(l\n)(n\Q\l) — 53(n\Q\n). (6.3)

For practical calculations, it is most convenient to choose the functions as eigenfunctions to the operator Q. If this is not possible we want to choose the functions at least as eigenfunctions of some dominant part of Q, so that the remainder is small in some sense. The precise meaning of small and how to choose the most appropriate functions to evaluate the respective traces will be discussed for special cases in later chapters of this book.

6.1 Ideal Fermi Gas

For didactic purposes, we write the spin index explicitly in this chapter. The Hamiltonian for a system of noninteracting Fermions is

H — 53 Ekak.sak.s — 53 EknKs , (6.4)

where Ek — h2k2/2m is the kinetic energy. The operators &k s and &k. s are, respectively, the creation and annihilation operators of a Fermion in the quantum state (k, s). They obey anti-commutation rules

and

(6.6)

see Appendix A. The combination

nk.s = al.sak.s (6.7)

is the particle number operator with the eigenstates |nk.s):

n-k.sln-k.s) = «k.s|«k.s) with nk.s =0, 1 , (6.8)

since each quantum state can be occupied by at most one Fermion.

To obtain the probability distribution function for Fermions, we compute the expectation value of the particle number operator in the state (k, s), i.e., we compute the mean occupation number

…. (e-9)

To evaluate these expressions, we use

This equation holds since the exponential operators on the LHS of Eq. (6.10) all commute, which directly follows from the commutation of the number operators for different states (k, s). Hence, Eq. (6.9) can be written as

Since the particle number operator is diagonal in the |nk.s) basis, we can use

in Eq. (6.11). It is most convenient to evaluate the trace with the eigenfunctions (6.8) of the particle number operator, so that

(6 12)

All factors (k', s') in the numerator and denominator of Eq. (6.11) cancel, except for the term with k' = k and sf = s. Therefore, Eq. (6.11) simplifies to

Evaluating the sums and rearranging the terms yields the Fermi-Dirac distribution

Fermi—Dirac distribution

Eq. (6.14) shows that the distribution function depends only on the magnitude of k and not on the spin. Therefore, we often denote the Fermi-Dirac distribution simply by fk. Examples for the Fermi-Dirac

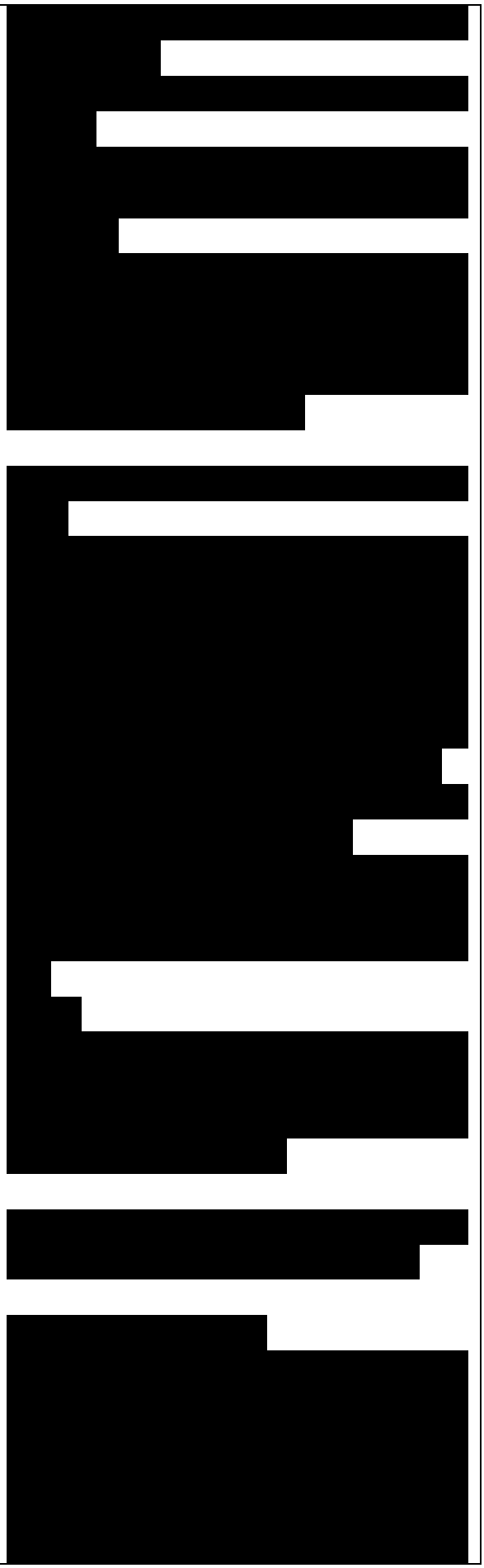

distribution function are plotted in Fig. 6.1 for three different temperatures.

We obtain the total number of particles N by summing the distribution function fk over all quantum states k, s:

N = £ fk = 2 £ fk . (6.15)

This relation determines the chemical potential ^ = fj,(n, T) as a function of particle density n and temperature T. In order to evaluate Eq. (6.15), it is again useful to convert the sum over k into an integral over the energy e

where, comparing to Eq. (4.7), the ^-dimensional density of states is identified as

6.1.1 Ideal Fermi Gas in Three Dimensions

For a system with three dimensions, Eq. (6.15) yields

(6.18)

Unfortunately, this integral cannot be evaluated analytically. We will therefore consider first the low-temperature limit T ^ 0 or 0 ^TO. If 0

fk = (0) for or fk = - e) , (6.19)

showing that the Fermi function degenerates into the unit-step function. The chemical potential of this degenerate Fermi distribution is often denoted as the Fermi energy Ep

(6.20)

where we have introduced kp as the Fermi wave number. This is the wave number of the energetically highest state occupied at T = 0. In this degenerate limit, Eq. (6.18) yields

(6'21)

Inserting this into Eq. (6.20), we get

(6.23)

In the high-temperature limit, where 0 ^ 0, the chemical potential must grow fast to large negative values

(6.24)

in order to keep the integral in Eq. (6.18) finite. The quantity exp(0^), called the virial, is thus a small quantity for 0Ep << 1 and can be used as an expansion parameter. In lowest approximation, the Fermi function can be approximated by

In this case, Eq. (6.18) yields

(6.26)

The integral is y/n/2, so that

(6.27)

where

(6'28)

or, using Eqs. (6.26) and (6.27),

(6 29)

Inserting this result into Eq. (6.25) yields the classical nondegenerate, or Boltzmann distribution

(6-3°)

Boltzmann distribution

For the parameters used in Fig. 6.1, the distribution function at T = 300K is practically indistinguishable from the Boltzmann distribution function (6.30) for the same conditions.

At this point, we will briefly describe how one can obtain an analytic approximation for fi(n,T), which is good for all except very strongly degenerate situations. Here, we follow the work of Joyce and Dixon (1977) and Aguilera-Navaro et al. (1988). According to Eq. (6.18), the normalized density v = n/no can be written as

. = - = 4= r,!,^ ae~J , (6.31)

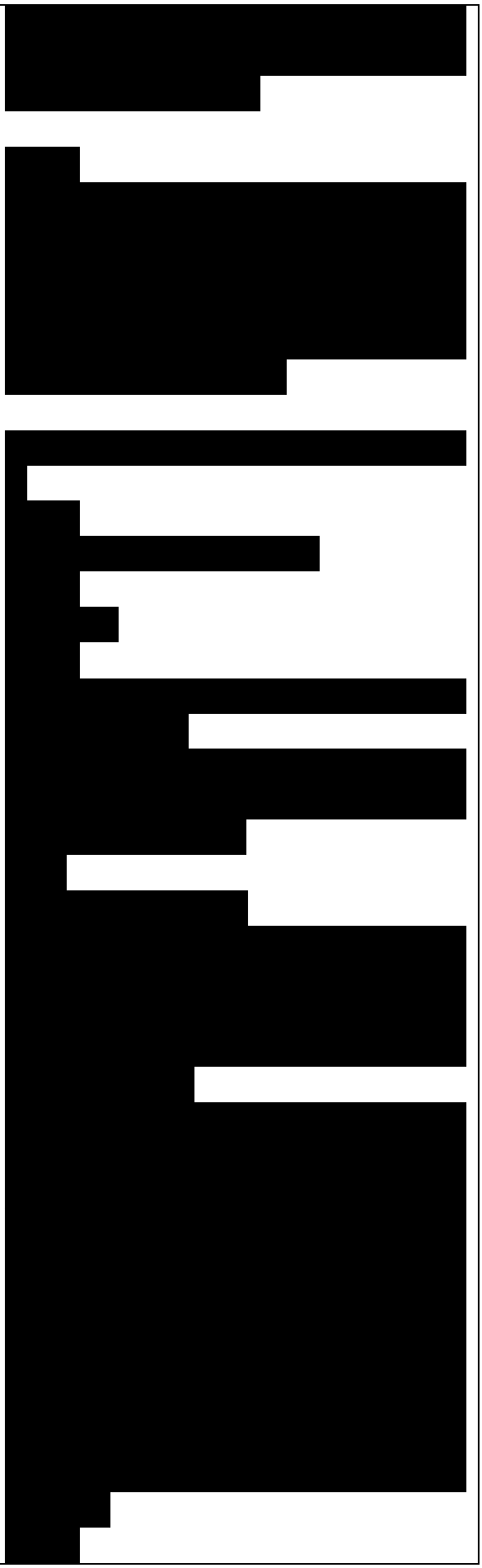

where z = exp(fi^). The integral can be evaluated using the series representation

Clearly, this expansion converges only for ^ < 0 or z < 1. However, the convergence range can be extended using the following resummation. First we invert Eq. (6.32) to express z in terms of v

where the comparison with Eq. (6.32) shows that bi = 1. Taking the logarithm of Eq. (6.33), we can write as

(6.34)

The logarithmic derivative of Eq. (6.34) yields

(6.35)

Now, we make a Pade approximation by writing the infinite sum on the RHS of Eq. (6.34) as the ratio of two polynomials of order L and M

This approximation is called the L/M-Pade approximation.

Comparison with the fully numerical result shows that the approximation with L = 2 and M = 1 already gives quite accurate estimates. A final integration yields

(6.37)

with K1 = 4.897, K2 = 0.045, and K3 = 0.133.

The comparison of Eqs. (6.37) and (6.29) shows that the logarithmic term in Eq. (6.37) is exactly the classical result. The chemical potential according to Eq. (6.37) is plotted in Fig. 6.2. Within drawing accuracy, the result is indistinguishable from the exact

chemical potential obtained as numerical solution of Eq. (6.18). Hence, Eq. (6.37) yields a good approximation for the range —tt < nfi < 30 .

6.1.2 Ideal Fermi Gas in Two Dimensions

For a two-dimensional system, Eq. (6.15) yields

where n = N/L2 now is the two-dimensional particle density and L2 is the area. Using exp(x) = t as a new integration variable, the integral in Eq. (6.38) becomes

(6.39)

Hence, we find the analytical result

n = —ln(l + e/3M) (6.40)

(6.41)

2D Fermion chemical potential

6.2 Ideal Bose Gas

Our discussion of the ideal Bose gas with spin s = 0 proceeds similar to the analysis of the ideal Fermi gas. The Hamiltonian is

and the Bose commutation relations are

(6.43)

and

[bk ,6k'] = [bl ,bl]=0 , (6.44)

see Appendix A. The expectation value of the particle number operator is

(6-45)

As in the Fermi case, the traces in Eq. (6.45) are evaluated choosing the eigenfunctions |nk) of the particle number operator

nk|nk) = nk|nk) , where nk = 0,1, 2,..., N,... TO . (6.46)

In contrast to the Fermi gas, where the Pauli principle allows all quantum states to be occupied only once, each state can be populated arbitrarily often in the Bose system. We obtain

(6.47)

where a = exp[—ft(Ek — j)]. It is straightforward to evaluate the numerator in Eq. (6.45) as derivative of the denominator, showing that Eq. (6.45) yields the Bose-Einstein distribution function

Bose-Einstein distribution

Generally, for Bosons we have two possible cases: 9 h 15

i) Particle number not conserved, i.e. N = ^2k gk = constant. In this case, j cannot be determined from this relation, it has to be equal to zero: j = 0.

Examples for this class of Bosons are thermal photons and phonons.

ii) Particle number conserved, i.e., N = ^kgk = constant. Then j = j(N,T) is determined from Eq. (6.15) as in the Fermi system. Due to the minus sign in the denominator of the Bose-Einstein distribution, the sum in Eq. (6.47) converges only for j < 0 since the smallest value of Ek is zero. Examples of this class of Bosons are He atoms.

In the remainder of this chapter, we discuss some properties of the Bose system with conserved particle number, case ii). As in the Fermi case, [j takes on large negative values for high temperatures. Thus, for T ^ TO, we can neglect the -1 in the denominator of Eq. (6.48) as compared to e-/3^ showing that the Bose-Einstein distribution also converges toward the Boltzmann distribution for high temperatures.

6.2.1 Ideal Bose Gas in Three Dimensions

If we study the chemical potential of the ideal Bose gas for decreasing temperatures, we find that j is negative and that its absolute value decreases toward zero. We denote the critical temperature at which j becomes zero as Tc :
j(n, T = Tc) =0 .

To determine the value of Tc, we use Eq. (6.48) with j = 0 and compute the total number of Bosons first for the three-dimensional system :
(6.50)

The series representation
(6.51)

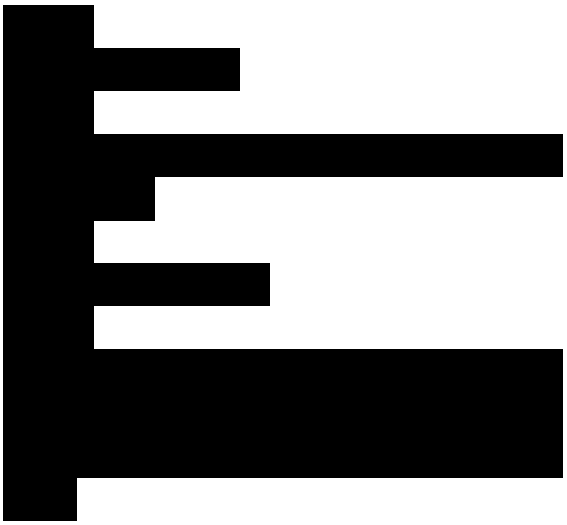

where the sum is the Z function and the integral is the r function, both with the argument 3/2. Hence, we obtain for the density

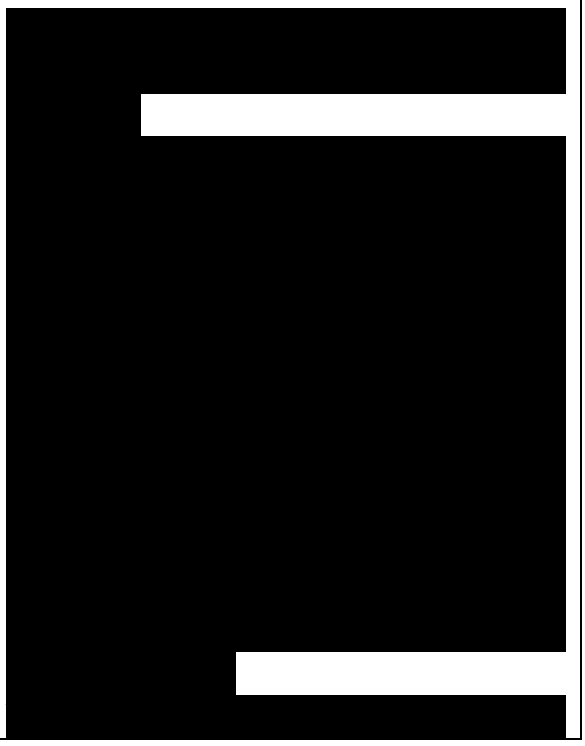

showing that n x T3/2 for fj, = 0. Setting T = Tc, i.e., p = pc, we find from Eq. (6.54) that
The result (6.55) implies that Tc is a finite temperature > 0. Now we know that fi = 0 at T = Tc, but what happens if T falls below Tc? The chemical potential has to remain zero, since otherwise the Bose-Einstein distribution function would diverge. All the calculations (6.50) - (6.54) assumed ^ = 0 and are therefore also valid for T < Tc. However, from the result (6.54) we see that N decreases with decreasing temperature yielding the apparent contradiction
The solution of this problem came

from the famous physicist Albert Einstein. He realized that the apparently missing particles in (6.56) are in fact condensed into the state k = 0, which has zero weight in the transformation from the sum to the integral in Eq. (6.16). Therefore, the term with k = 0 has to be treated separately for Bose systems at T <Tc. This can be done by writing

This equation shows that all particles are condensed into the state k =0 at T = 0. This condensation in k-space is called the Bose-Einstein condensation. It corresponds to a real-space correlation effect in the Bosonic system leading to superconductivity and superfluidity. For temperatures between T = 0 K and Tc, the three-dimensional Bose system consists of a mixture of condensed and normal particles.

6.2.2 Ideal Bose Gas in Two Dimensions

Using the two-dimensional density of states, we get for the total number of Bosons

(6.58)

The resulting expression for the two-dimensional particle density, n = N/L2, can be evaluated in the same way as the corresponding expression for Fermions, yielding

(6.59)

The argument of the logarithmic term has to be larger than 0, i.e., e<1 and fi < 0 for any finite f3 value. Therefore, the chemical potential approaches zero only asymptotically as T ^ 0 and there is no Bose-Einstein condensation in an ideal two-dimensional Bose system.

6.3 Ideal Quantum Gases in D Dimensions

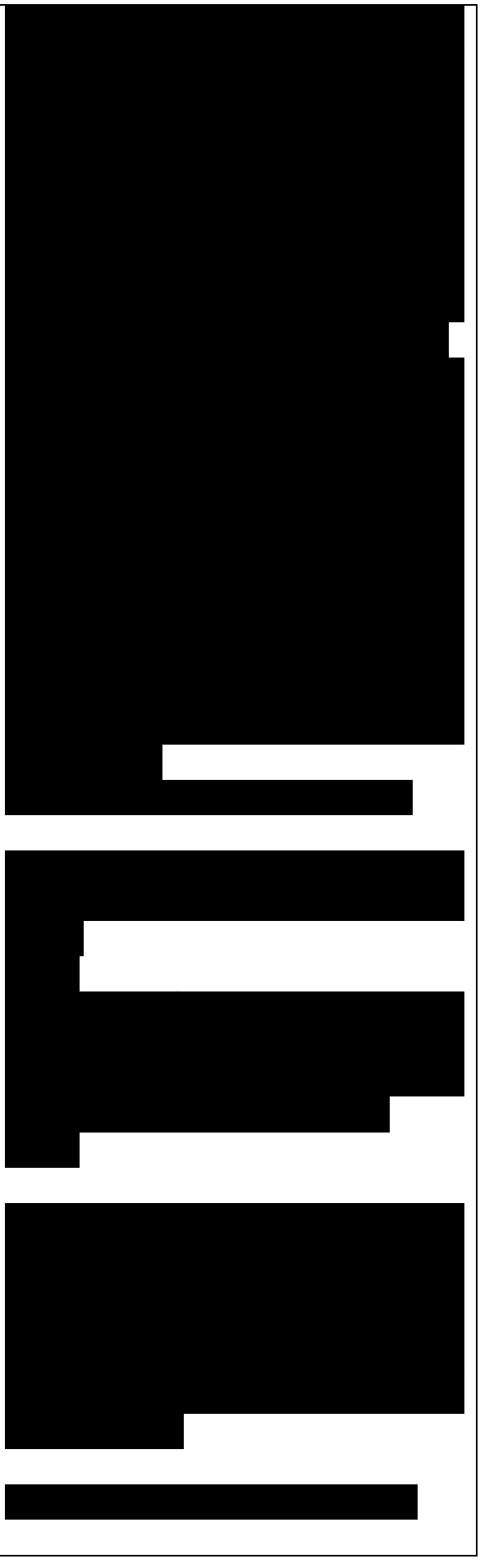

In this section, we summarize some universal results for the temperature and density dependence of the chemical potential for Fermi, Bose, and Boltzmann statistics in a P-dimensional ideal quantum gas. In the previous sections, we have already considered the three- and two-dimensional cases.

Here, however, we also include the one-dimensional case and formalize the previous considerations.

As discussed preceding Eq. (6.15), the chemical potential i is determined from the relation

(6.60)

where n = N/LD is the ^-dimensional particle density, 2s + 1 is the spin degeneracy, with s = 0 or 1 for Bosons and s = 1/2 for Fermions, and k is the ^-dimensional wave vector. The thermal distributions f± are defined as

ft= e,3(Ek-»)± i > (6.61)

with + for Fermions and — for Bosons. As before, we reformulate Eq. (6.60) with the virial z = e^^ and get

(6.63)

The first factor ID(0) in Eq. (6.62) can be evaluated most easily in Cartesian coordinates:

-(*)-•(©. <«*> where the ^-dimensional zero-point energy is

(6.65)

The ^-dimensional integrals of the final normalized expression I±(z)/ID (0) in Eq. (6.62) are now evaluated in polar coordinates. Because the integrands do not depend on angles, the space angle as well as other normalization constants drop out and we obtain from Eq. (6.62) :

(6.66)

where
The gamma function is given for D = 3, 2, and 1 by the values r(3/2) = v^/2, r(i) = i,r(i/2) = a/7t, respectively. In general, the integral Jp(z) has to be evaluated numerically for the three- and one-dimensional cases. We obtain an analytical result only in two dimensions (see Sec. 6-1.2 and 6-2.2):
As before, the limiting case of Boltzmann distributions is obtained from Eq. (6.66) if we approximate the factor J±(z)/JD(0) ^ 1.

In order to compare the particle statistics with each other for different dimensionalities, we rewrite Eq. (6.66) as
The ratio of the thermal energy kBT to the zero-point energy EOD is a measure of the degeneracy of the ideal quantum gas. For ratios larger than one, quantum effects can be neglected. On the other hand, quantum effects dominate over thermal ones if kBT/EOD is smaller than one. In Fig. 6.3, we plot kB T/EOD logarithmically versus the ratio of the chemical potential to the thermal energy if. For better comparison, we have put s = 0 for all cases. In such a plot, we obtain a straight line with a slope of -2/D for the Boltzmann limit, as can be seen by taking the logarithm of the RHS of Eq. (6.69).

For Bosons, the figure shows clearly that for D = 3 the chemical potential becomes zero in the vicinity of kBT ^ EOD, whereas it approaches zero

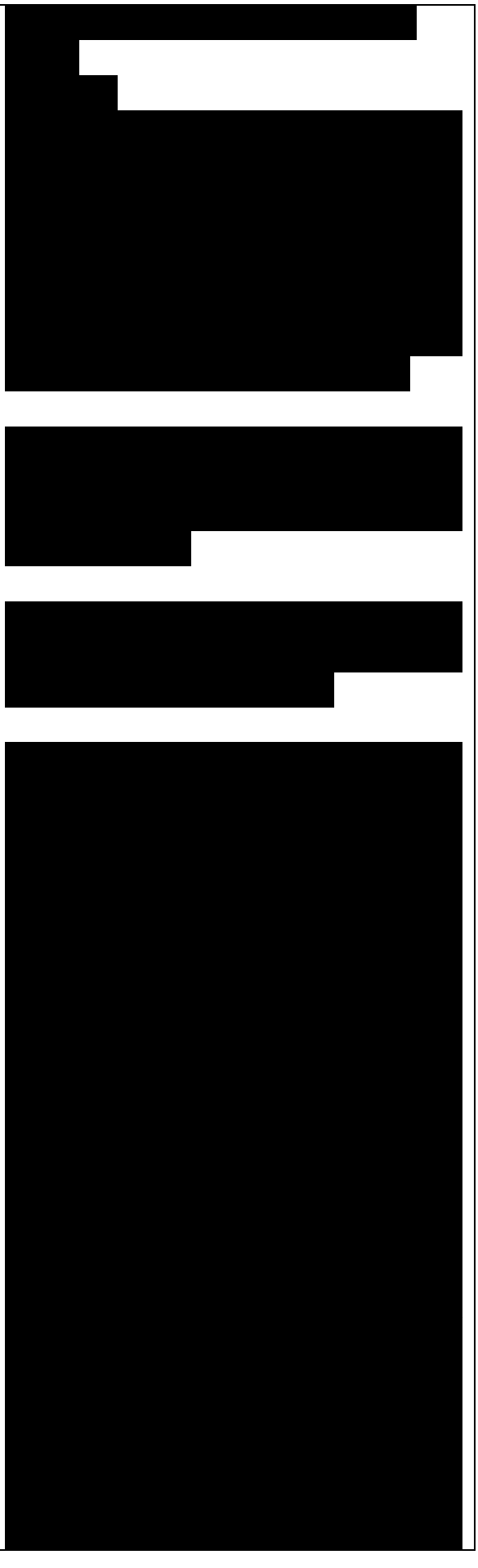

only asymptotically for D = 2,1. This shows again the absence of a Bose-Einstein condensation in dimensions lower than three. For Fermions, the chemical potential becomes positive and converges to the Fermi energy as the degeneracy parameter kB T/EOD ^ 0.

Fig. 6.3 Comparison of kBT/EQD plotted logarithmically versus ^0 for the Bose, Fermi and Boltzmann statistics of a 3D, 2D and 1D quantum gas.

PROBLEMS

Problem 6.1: Consider a linear chain of atoms with masses M and interatomic distance a. The coupling between the atoms is given by a harmonic force with the force constant K.

a) Show that the Lagrange function is
where qr is the displacement of the r-th atom from its equilibrium position.

b) Compute the canonical momentum pr.

c) The displacements can be expanded into normal coordinates Qk
qr(t) = ^£Qk(t)eikar .
Use
£eiar(k-k"> = NSkk' k
and the periodic boundary conditions qr+N = qr to determine the allowed fc-values.

d) The displacements are quantized by introducing the commutation relations
Use the fact that the displacement is a Hermitian operator to show the relations
and

e) Introduce the phonon operators dk and d\ through the linear transformations

Verify the phonon commutation relation

and show that the Hamiltonian becomes

Hint: Follow the discussion in Appendix A.

Problem 6.2: The Fourier expansion of A is given by

and correspondingly for n(r,t). Prove, that in the Coulomb gauge the commutator of A(k,t) and n(k,t) is

Problem 6.3: Expand the chemical potential of a nearly degenerate 3D Fermion system for low temperatures (Sommerfeld expansion).

Problem 6.4: Determine the temperature at which a 2D Fermion system of a given density has zero chemical potential.

Problem 6.5: Calculate the energy and specific heat of a nearly degenerate 2D Fermion system.

Chapter 7

Interacting Electron Gas

In this chapter, we discuss a model for the interacting electron gas in a solid. To keep the analysis as simple as possible, we neglect the discrete lattice structure of the ions in the solid and treat the positive charges as a smooth background, called jellium-like jelly.

This jellium model was originally designed to describe the conduction characteristics of simple metals. However, as we will see in later chapters of this book, this model is also useful to compute some of the intraband properties of an excited

semiconductor. In such a system, we have to deal with an electron-hole gas, which consists of the excited electrons in the conduction band and the corresponding holes, i.e., missing electrons, in the valence band. In this case, one again has total charge neutrality, since the negative charges of the electrons are compensated by the positive charges of the holes.

In the following sections, we discuss the jellium model in such a way that only very minor changes are required when we want to apply the results to the case of an excited semiconductor.

7.1 The Electron Gas Hamiltonian

The Hamiltonian of a three-dimensional electron system is the sum of kinetic and interaction energy. In the previous chapter on ideal quantum gases, we discussed the kinetic energy part in great detail. Now we add the Coulomb interaction part in the jellium model approximation. For this purpose, we write the Coulomb Hamiltonian in first quantization as
(7.1)

where W is the interaction potential. Since the detailed form of W is not needed for our initial considerations, we defer this discussion until the end of this section. The term r = r' has to be excluded from the integration in (7.1) since this is the infinite interaction energy of charges at the same position (self-energy). For notational simplicity, we keep the unrestricted integration and subtract the self-energy at the end.

The index a in Eq. (7.1) runs over electrons, a = e, and ions, a = i. The charge density pa is

(7.2)

for the electrons and

(7.3)

for the ions, reflecting our assumption that the ions form a uniform positive charge background.

Now, we take the Fourier transformation of the charge density and the interaction potential. For the spatial 3D Fourier transformation, we use the following conventions

(7.4)

(7.5)

(7.6)

(7.7)

With these definitions we obtain the Coulomb interaction Hamiltonian

(7.1)

where

(7-9)

(7.10)

Evaluating the sum over electron and ion contributions allows us to write the total Coulomb Hamiltonian as the sum of three terms:

(7.11)

The electron-electron interaction is

(7.12)

where we separated the contribution with q = 0 in the second line. For the electron-ion interaction, we get

(7.13)

and the ion-ion interaction yields

(7.14)

Adding all the contributions (7.12) - (7.14), we obtain for the Coulomb Hamiltonian in the jellium model

(7-15)

In the double summation, we now exclude the term with i = j, which is just the electron self-interaction mentioned in the discussion after Eq. (7.1). Writing

and using (7.9), the Coulomb Hamiltonian becomes

Coulomb Hamiltonian for jellium model

The calculations leading to the Hamiltonian (7.17) show that the only, but extremely important effect resulting from the attractive interaction of the electrons with the homogeneous positive charge background is to eliminate the term q = 0 from the sum in the electron-electron interaction Hamiltonian.

In order to obtain the Coulomb Hamiltonian in second quantization, we replace the charge density peq in (7.17) by the charge density operator

Pe,-q ^ pe,-q : (7.18)

and

(7.19)

where N is the operator for the total number of electrons, so that

As the next step, we now want to introduce the electron creation and destruction operators a£ s and Nk,s, which we used already in Chap. 6. For this purpose, we write the charge density operator in real space as

pe(r) = —\e\ n(r) = -\e\ E V>st(r)Vs(r) , (7.21)

where the field operators VS(r), ips(r) describe creation and destruction of an electron at position r with spin s (see Appendix A). Using the plane-wave expansion

, (7.22)

we obtain

= -JJ E 'V,"-' k k " • (7-23)

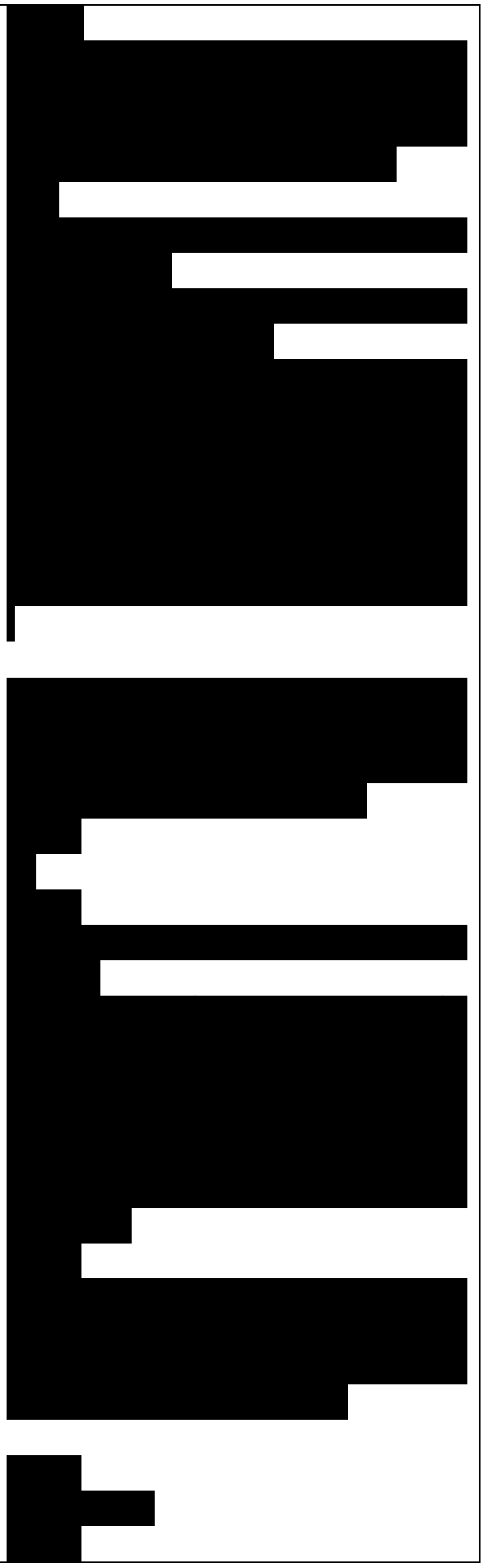

Taking the Fourier transformation of (7.23) yields

Pe,1 = ~ Jji 53 ®k-q,s®k>s • (7.24)

After inserting (7.24) into the Hamiltonian (7.20), we obtain

Wc = J E "k <,."k.-'V - J E^ > (7-25)

where we abbreviated

Vq = e2Wq . (7.26)

Reordering the creation and destruction operators using the anticommutation relations (6.5) - (6.6) yields

(7.27)

The last two terms cancel since

(7.28)

Adding the kinetic energy part, Eq. (6.4), we obtain the total electron gas Hamiltonian

(7.29)

electron gas Hamiltonian

The only missing ingredient is now the detailed form of the interaction potential Vq. We start from the Coulomb interaction potential in real space

(7.30)

where we include the background dielectric constant eo to take into account the polarizability of the valence electrons and of the lattice. Using Eq. (7.4), we have

(7.31)

To evaluate the remaining integral in Eq. (7.31), we introduce the convergence generating factor exp(—■jr) under the integral and take the limit of

Y ^ 0 after the evaluation. This yields

(7.32)

3D Coulomb potential

7.2 Three-Dimensional Electron

Gas

Now we use the electron gas Hamiltonian to compute the ground-state energy (T = 0) in Hartree-Fock approximation. Since we know that at T = 0 all particles are in states with \k\ < kF, the Hartree-Fock ground-state wave function is

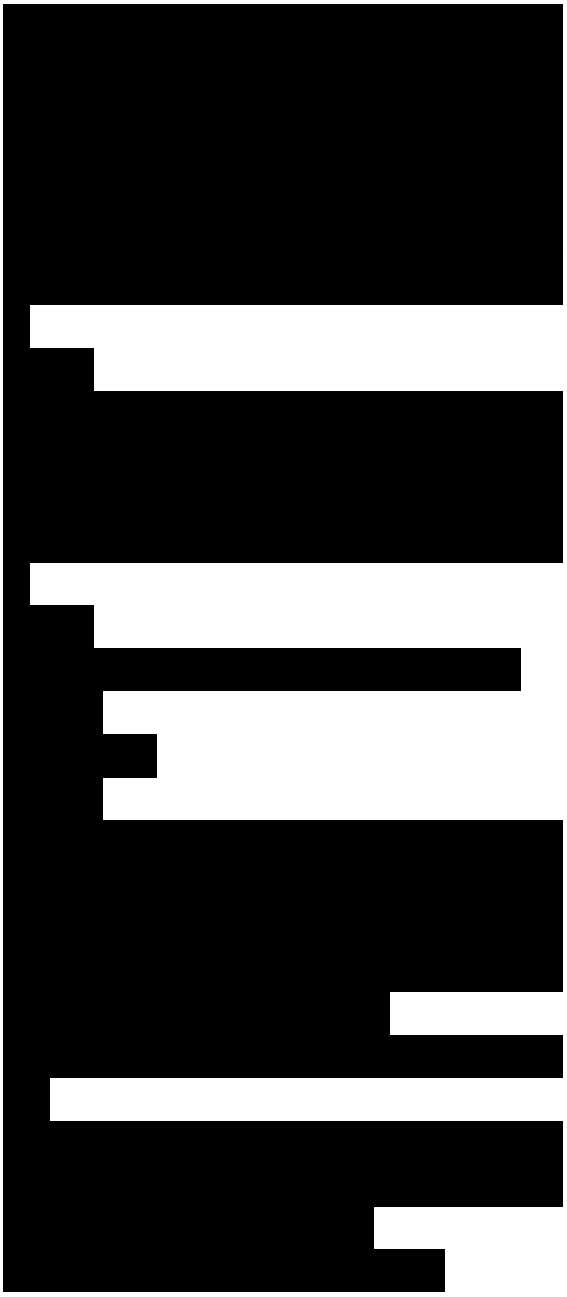

(7.34)

Due to the anti-commutation relations between the Fermi operators, Eq. (7.34) automatically has the correct symmetry. The Hartree-Fock ground state energy is

(7.35)

First we evaluate the kinetic energy

(7.36)

We simply get

(7.37)

since in the Hartree-Fock ground state all states below the Fermi wave number are occupied and all states above kF are empty. The 0-function can also be written as

which is just the Fermi distribution at T = 0. Therefore,

where Eq. (4.6) for D = 3 has been used. With the Fermi wave number kF = (3n2n)1/3, Eq. (6.22), we find

For the potential energy, we obtain

(7.41)

This term is nonzero only if

(7.42)

as can be seen by acting with the destruction operators on the Hartree-Fock ground state to the right, and with the h.c. of the creation operators on the Hartree-Fock ground state to the left, respectively. To evaluate (7.41), we now commute ak'-q s' to the right, using the Fermi commutation relations repeatedly. We

obtain

(7.43)

where q = 0 and

(7.44)

has been used. Furthermore,

(7.45)

since all states |k + q| < kF are occupied. Using (7.42) - (7.45) and inserting into (7.41) yields

(7.46)

Explicit evaluation of the sum in the last line and use of Eq. (6.22) gives (see problem 7.1)

(7-47)

The Hartree-Fock result for the potential energy due to electron-electron repulsion is just the exchange energy, which increases with density with a slightly smaller power than the kinetic energy. The exchange energy is an energy reduction, since the term with q = 0 is omitted from the Hamiltonian as a consequence of the Coulomb attraction between electrons and positive jellium background. Adding Eqs. (7.40) and (7.47) we obtain the total Hartree-Fock energy as

(7'48)

For low densities, the negative exchange energy dominates, while the kinetic energy is larger at high densities, see Fig. 7.1. For intermediate densities, there is actually an energy minimum, indicative of the existence of a stable phase which is the electron-hole-liquid phase. Hence, already at the level of this relatively simple Hartree-Fock theory, we find signatures of a stable electron-hole liquid. This famous prediction of Keldysh has been verified experimentally by the

observation of electron-hole liquid droplets, mostly in indirect gap semiconductors. The density within these droplets is the stable liquid density. They condense and coexist with the electron-hole gas, as soon as a critical density is exceeded and the temperature is below the critical condensation temperature.

In order to gain more physical insight into electron gas properties and to understand the energy reduction due to the exchange effects, we now calculate for the Hartree-Fock ground state the conditional probability to simultaneously find electrons at the position r with spin s and at v' with

Fig. 7.1 Hartree-Fock energy versus density scaled by the Bohr radius ao = heo/(me2)

spin s'. This conditional probability is just the correlation function

(7.49)

Obviously, this correlation function is only finite if the annihilation operators simultaneously find an electron in (r, s) and (r', s'). The creation operators simply put the annihilated electrons back into their previous states.

Using (7.22) to express the field operators in terms of the electron creation and destruction operators allows us to write the electron correlation function as

(7.50)

The sum runs over (l, l', k, k') with (|l|, |l'|, |k|, |k'|) < kF. As in our calculation of EHJt, we again commute all creation operators to the right and use Eq. (7.44). As intermediate step, we obtain

(7.51)

where the first term is the so-called direct term and the second term is the exchange term. Using the Fermi anti-commutation relations and Eq. (7.44) one more time yields
The first term in (7.52) results from
where we have to divide the total electron number N by two since no spin summations are included, and in the second term we defined

Here, we used Eq. (6.22) to introduce the factor kp in terms of the density n. Inserting Eq. (7.53) into Eq. (7.52), we obtain
(7.54)

This result is plotted in Fig. 7.2. It shows that the conditional probability to find an electron at r' with spin s', given that there is an electron at r with spin s, depends only on the separation |r — r'| between the two electrons. Furthermore, if s and s' are different, the second term on the RHS of Eq. (7.54) vanishes, and we find that the correlation function is constant. However, for electrons with equal spin, s = s', we can convince ourselves by a Taylor expansion that Rss(p ^ 0) ^ 0. This result shows that the electrons with equal spin avoid each other as a consequence of the Pauli exclusion principle (exchange repulsion). Each electron is surrounded by an exchange hole, i.e., by a net positive charge distribution.

The existence of the exchange hole expresses the fact that the mean separation between electrons with equal spin is larger than it would be without the Pauli principle. This

result is correct also for the ideal Fermi gas, where actually the Hartree-Fock ground state is the exact ground state of the system. For the interacting electron gas treated in this chapter, the increased separation between repulsive charges reduces the overall Coulomb

Fig. 7.2 Pair correlation function Rssi for the three-dimensional electron plasma, Eq. (7.54), as function of the dimensionless particle distance kpp, where p = |r — r'\ and kp is given by Eq. (6.22).

repulsion. One can say that the electron interacts with its own exchange hole. Since this is an attractive interaction, the total energy is reduced, as we found in Eq. (7.47).

According to the Hartree-Fock theory, electrons with different spin do not avoid each other, since the states are chosen to satisfy the exchange principle but they do not include Coulomb correlations. The exchange principle is satisfied as long as one quantum number, here the spin, is different. However, in reality there will be an additional correlation, which leads to the so-called Coulomb hole. To treat these correlation effects, one has to go beyond Hartree-Fock theory, e.g., using screened Hartree-Fock (RPA), see Chap. 9. Generally, one can write the exact ground state energy E0 as

E0 — E0)F + Ecor — EHF + Eexc + Ecor , (7.55)

where the correlation energy is defined as

Ecor — E0 — E0/F . (7.56)

An exact calculation of Ecor is generally not possible. To obtain

good estimates for Ecor is one of the tasks of many-body theory.

7.3 Two-Dimensional Electron Gas

Even in those semiconductor structures which we consider as lowdimensional, such as quantum wells, quantum wires, or quantum dots, the Coulomb potential varies as 1/r. The reason is that the electric field lines between two charges are not confined within these structures. The field lines also pass through the surrounding material, which is often another semiconductor material with a very similar dielectric constant.

In this section, we discuss the situation of idealized semiconductor quantum wells, where the electron motion is confined to two dimensions, but the Coulomb interaction has its three-dimensional space dependence. For simplicity, we disregard here all modifications which occur for different dielectric constants in the confinement layer and the embedding material. As introduced in Chap. 4, we assume that the carriers are confined to the x, y layer and put the transverse coordinate z = 0. For this case, we need only the two dimensional Fourier transform of the Coulomb potential:

^ = I ^V(r)e^ (7.57)

with V(r) given by Eq. (7.30). Eq. (7.57) yields

where Jo(x) is the zero-order Bessel function of the first kind. Since

we obtain

(7.59)

quasi- 2D Coulomb potential

Eq. (7.59) shows that the Coulomb

potential in two dimensions exhibits a 1/q dependence instead of the 1/q2 dependence in 3D.

In the evaluation of the pair correlation function RsS (r, r') for the 2D electron gas, we obtain formally the same result as in Eq. (7.52), except now

with Ji being the first-order Bessel function of the first kind. Here we have introduced the two-dimensional Fermi wave number kp through the relation

(7.68)

Evaluating Eq. (7.68) yields

(7.69)

The resulting pair correlation function for 2D is plotted in Fig. 7.3. Schematically, the variations of the correlation function in two-dimensions resemble those of the three-dimensional result shown in Fig. 7.2. A more detailed comparison between Figs. 7.2 and 7.3, however, shows that the oscillatory structures are somewhat more pronounced in the 2D system, indicating that the exchange correlations of the electrons are stronger in two than in three dimensions.

7.4 Multi-Subband Quantum Wells

In order to calculate the properties of electron gases in quantum wells with several subbands, we have to evaluate the matrix elements of the Coulomb potential between the various envelope eigenfunctions of the quantum well. It is convenient to start with the 3D Fourier transform of the Coulomb potential VqD of Eq. (7.33), where L3 has to be replaced by L?Lz

with Lz being the thickness of the quantum well. With this modification, we obtain the Coulomb potential Vq\\(z), where z is the coordinate perpendicular to the layer, by a 1D Fourier transform of Eq. (7.33) with respect to the perpendicular momentum component q± :

where we have split the momentum vector into its components parallel and perpendicular to the plane. With Aq^ = 2n/Lz we get

The Coulomb potential of a quasi-2D structure, Eq. (7.59), follows from this general result in the limit qnN << 1.

The matrix elements of the Coulomb interaction Vq^ (zi — Z2) between two electrons at the perpendicular positions zi and Z2 described by the envelope functions Qn(zi) are

(7.72)

Coulomb potential for multi-band quantum wells

The interaction Hamiltonian in the multi-subband situation is

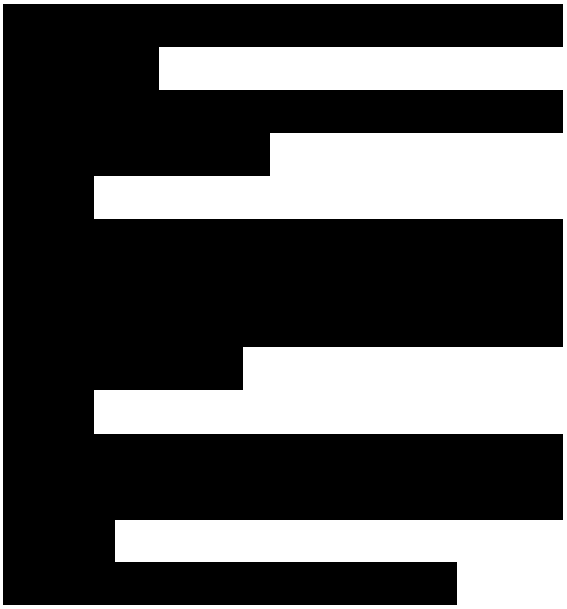

(7.73)

Here, the vectors k, k', q are all momentum wave vectors in the plane of the quantum well. The resulting exchange energy is

(7.74)

where fm,k is the occupation probability of state m, k and the term q = 0 has to be excluded.

7.5 Quasi-One-Dimensional Electron Gas

Motivated by the success of semiconductor quantum-well structures in permitting the study of quasi-two-dimensional phenomena, there is strong interest in structures with even more pronounced quantum confinement effects. Examples are the

quantum wires where electrons and holes are free to move in one space dimension, and the quantum dots where the carriers are confined in all three space dimensions. Quantum dots will be discussed separately later in this book.

In this section, we analyze some of the basic physical properties of electrons in quantum wires. Quantum wires have been made in different sophisticated ways, always adding quantum confinement to restrict the free carrier motion to one dimension. The additional confinement potentials have been generated through various techniques, such as growth of structures on specially prepared substrates, using grooves, etching of quantum wells, ion implantation, or with the help of induced stresses in the material below a quantum well.

The analysis of the confinement effects in quantum wires has to be done carefully. If we simply put the transverse coordinates $x = y = 0$, we would find that the resulting one-dimensional Coulomb potential has several pathological features. Loudon showed already in the year 1959 that the ground-state energy of an electron-hole pair is infinite in one dimension.

In order to obtain a regularized Coulomb potential, we consider a quasi- one-dimensional quantum wire with a finite but small extension in the quantum-confined directions. We use the envelope function approximation for the carrier wave functions and average the Coulomb potential with the transverse

quantized envelope functions. This way, we obtain a mathematically well-defined, nonsingular interaction potential. The simplest example is a cylindrical quantum wire of radius R with infinite lateral boundaries. For this case, the envelope wave function corresponding to the lowest confinement energy level is

(7'75)

where Jn(p) is the radial Bessel function of order n. The corresponding confinement energy is

and ao = 2.405 is the first zero of J0(x) = 0. The denominator in Eq. (7.75) results from the normalization of the wave function (see problem 7.3).

The quasi-one-dimensional (q1D) Coulomb potential between two electrons is obtained by averaging the three-dimensional Coulomb potential with the radial envelope functions :

(7.77)

quasi-1^ Coulomb potential

This quasi-one-dimensional Coulomb potential is finite at z = z\ — Z2 = 0 and can be approximated quite well by the simple regularized potential

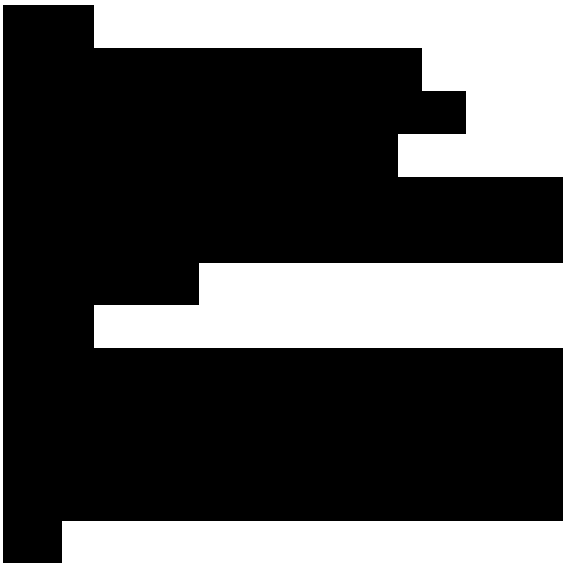

(7.78)

where 7 is a fitting parameter which has the value 7 ~ 0.3. As shown in Fig. 7.4, the potential (7.78) is finite at z = 0, and varies as 1/z for large distances.

From Eq. (7.46) we see that the quasi-one-dimensional exchange energy for a thermal electron gas is

(7-79)

where Vjq1D is the Fourier transform with respect to z of (7.77) or its approximation (7.78). At T = 0, Eq.

(7.79) yields (7.80) and the one-dimensional density is PROBLEMS Problem 7.1: Use the Hamiltonian (7.29) and the Hartree-Fock wave function (7.34) to compute the ground-state energy with the 3D and the 2D Coulomb interaction potentials, respectively. Hint: Use the expansion in terms of Legendre polynomials and the integrals = 0 for n odd .	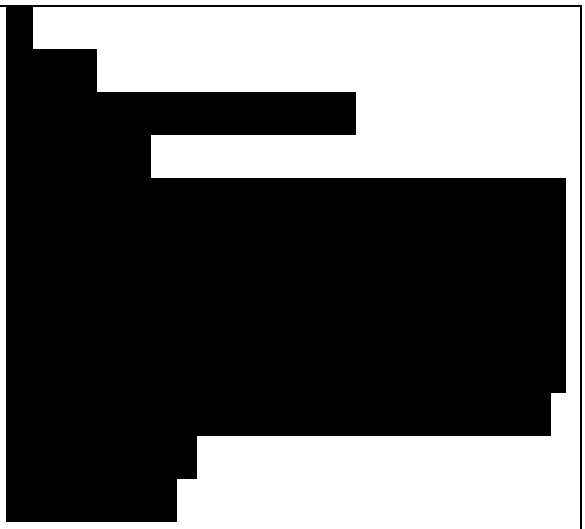

Using Eq. (7.59) in Eq. (7.46), we obtain the exchange energy as (see problem 7.1) (7.60) where (7.61) is a numerical constant and n = N/L2. In order to compare the exchange energy in 2D and 3D, we introduce the normalized distance rs between particles through the relation (7.62) in 3D. Here, ao is the characteristic length scale given by the Bohr radius of the bound electron-hole pairs, i.e., excitons (see Chap. 10 for details). At this point we use the definition of ao as (7.63) in three dimensions. In two dimensions, we have (7.64) where ao now is the 2D Bohr radius, which is half of the 3D Bohr radius. The 3D exchange energy is seen to vary with the particle distance rs as (7.65) whereas (7.66) i.e., in three dimensions the exchange energy falls off more rapidly for larger distances than in two dimensions. This is a consequence of the larger phase space volume for D = 3 compared to the D = 2 case.	Dùng Pt. (7.59) trong PT. (7.46), chúng ta thu được năng lượng trao đổi dưới dạng (xem bài tập 7.1) (7.60) Trong đó (7.61) Là hằng số và n = N/L2. Để so sánh năng lượng trao đổi trong trường hợp 2 chiều và 3 chiều, chúng ta đưa vào khoảng cách chuẩn hóa rs giữa các hạt thông qua hệ thức (7.62) Trong không gian 3 chiều. Ở đây, ao là thang chiều dài đặc trưng theo bán kính Bohr của cặp electron-lỗ trống liên kết, chẳng hạn., excitons (xem Chap. 10 để tìm hiểu kỹ hơn). Vào lúc này, chúng ta dùng định nghĩa của ao là (7.63) Trong trường hợp ba chiều. Trong trường hợp hai chiều, chúng ta có (7.64) Lúc này ao là bán kính Bohr 2 chiều, băng phân nửa bán kính Bohr 3 chiều. Chúng ta thấy nằng lượng trao đổi 3 chiều thay đổi theo khoảng cách hạt dưới dạng (7.65) Miễn là (7.66) Tức là, trong không gian ba chiều, năng lượng trao đổi ở khoảng cách lớn giảm nhanh hơn so với trong trường hợp hai chiều. Đây là hệ quả cửa việc thể tích pha không gian đối với trường hợp D=3 lớn hơn trường hợp D=2.

Dịch hình

Fig. 4.1 The full lines show the mixing of the heavy and light-hole valence bands in a GaAs quantum well according to Eq. (4.36). The thin lines show the bands without band mixing.	H.4.1 Các đường đậm nét thể hiện sự pha trộn giữa các vùng hóa trị lỗ trống nặng và nhẹ trong giếng lượng tử GaAs theo Pt.(4.36). Các đường mảnh biểu diễn các vùng không có sự pha trộn.
Fig. 5.1 Schematic drawing of conduction and valence bands and an optical dipole transition connecting identical k-points in both bands.	H.5.1 Biểu diễn sơ đồ các vùng dẫn và vùng hóa trị và dịch chuyển lưỡng cực quang kết nối các điểm k giống nhau ở cả hai vùng.
Fig. 5.2 Schematic drawing of the rotation of the Bloch vector for excitation with a rectangular pulse of area n/2 pulse and a finite detuning for T2 ^ Ti.	H.5.2.Biểu diễn quá trình quay vector Bloch để kích thích với một xung hình chữ nhật có diện tích n/2 và độ lệch hưởng hữu hạn đối với T2 ^ Ti.
Fig. 5.3 Free electron absorption spectra for semiconductors, where the electrons can move freely in one, two, or three space dimensions.	Hình 5.3 Phổ hấp thụ electron tự do của các chất bán dẫn, trong đó các electron có thể di chuyển tự do trong không gian một, hai hoặc ba chiều.
Fig. 5.4 Absorption/gain spectra for a one-dimensional free carrier system using the carrier densities N = 0, 3.5, 5.4, 7.4 x 105cm_ 1, from top to bottom.	H.5.4 Phổ hấp thụ/độ lợi của hệ hạt tải điện tự do một chiều dùng mật độ hạt tải N = 0, 3.5, 5.4, 7.4 x 105cm_ 1, từ đỉnh đến đáy.
Fig. 5.5 Absorption/gain spectra for a two-dimensional free carrier system using the carrier densities N = 0, 5, 8.3, 12 X 1011 cm-2, from top to bottom.	Hình 5.5 Phổ hấp thụ/độ lợi của hệ hạt tải điện tự do hai chiều dùng mật độ hạt tải N = 0, 5, 8.3, 12 X 1011 cm-2, từ đỉnh đến đáy.
Fig. 5.6 Absorption/gain spectra for a three-dimensional free carrier system using the carrier densities N = 0, 3.3, 5.8, 9.5 X 1017cm~3, from top to bottom.	H 5.6 Phổ hấp thụ/độ lợi của hệ hạt tải ba chiều dùng mật độ hạt tải N = 0, 3.3, 5.8, 9.5 X 1017cm~3, từ đỉnh đến đáy.
Fig. 6.1 Fermi—Dirac distribution function fk as function of Ek/kB for the particle density n = 1 • 1018cm-3 and three temperatures.	H.6.1 Hàm phân bố Fermi-Dirac fk theo Ek/kB ứng với mật độ hạt n = 1 • 1018cm-3 và ba nhiệt độ.

Fig. 6.2 Chemical potential fi for a three-dimensional Fermi gas as function of n/no where no is defined in Eq. (6.28).	Hình 6.2 Thế hóa học fi đối với khí Fermi ba chiều theo n/no Trong đó no được định nghĩa theo phương trình (6.28).
Fig. 6.3 Comparison of kBT/EQD plotted logarithmically versus ^0 for the Bose, Fermi and Boltzmann statistics of a 3D, 2D and 1D quantum gas.	Hình 6.3 So sánh đồ thị logarit theo ….của các thống kê Bose, Fermi và Boltzmann đối với khí lượng tử 3 chiều, 2 chiều và một chiều.
Fig. 7.1 Hartree-Fock energy versus density scaled by the Bohr radius ao = heo/(me2)	H. 7.1 Năng lượng Hartree-Fock theo mật độ được lấy tỷ lệ theo bán kính Bohr ao = heo / (Me2)
Fig. 7.2 Pair correlation function Rssi for the three-dimensional electron plasma, Eq. (7.54), as function of the dimensionless particle distance kpp, where p = |r — r'\ and kp is given by Eq. (6.22).	H.7.2 Hàm tương quan cặp Rssi của plasma electron ba chiều, Pt (7.54), theo khoảng cách hạt không thứ nguyên kpp, trong đó p = |r — r'\ và kp đã được định nghĩa trong Pt (6.22).
Fig. 7.3 Pair correlation function Rss' for the quasi-two-dimensional electron plasma, Eqs. (7.52) and (7.67), as function of the dimensionless particle distance kFp, where p = |r — r'\ and kF is given by Eq. (7.69).	H.7.3 Hàm tương quan cặp Rss' của plasma electron giả hai chiều, Pt (7.52) và (7.67), theo khoảng cách hạt không thứ nguyên kFp, trong đó p = |r — r'\ và kp đã được định nghĩa trong Pt (7.69).
Fig. 7.4 The quasi-one-dimensional Coulomb potential according to Eq. (7.77) as func¬tion of particle separation z (thick solid line). The dashed curve is a Coulomb potential, and the thin solid line is the regularized Coulomb potential, Eq. (7.78), for 7 = 0.3.	H.7.4 Thế Coulomb giả một chiều theo Pt (7.77) như một hàm theo khoảng cách hạt z (đường liền nét). Đường nét đứt là thế Coulomb, và đường liền nét là thế Coulomb chính tắc, Pt (7.78), khi …..